CRYSTAL GROWTH & DESIGN

pubs.acs.org/crystal

Article

Structural Landscape of Zn(II) and Cd(II) Coordination Compounds with Two Isomeric Triimidazole Luminophores: Impact of Crystal Packing Patterns on Emission Properties

Marina S. Fonari,* Victor C. Kravtsov, Victor Bold, Elena Lucenti, Elena Cariati,* Daniele Marinotto, and Alessandra Forni

Cite This: https://doi.org/10.1021/acs.cgd.1c00459

Read Online

ACCESS | Metrics & More | Article Recommendations | Supporting Information

ABSTRACT: The interplay of different Zn(II) and Cd(II) salts with two luminescent triimidazole ligands, triimidazo[1,2-*a*:1′,2′-*c*:1″,2″-*e*][1,3,5]-triazine (L_1) and its positional isomer triimidazo[1,2-*a*:1′,2′-*c*:1″,5″-*e*][1,3,5]triazine (L_2), in solvothermal synthetic conditions resulted in mono-, bi-, and polynuclear Zn(II) and Cd(II) coordination compounds with diverse metal/luminophore(L_1,L_2)/anion/water ratios, $[Zn(H_2O)_6](NO_3)_2(L_1)_2$ (**1**), $[Zn(H_2O)_4(L_1)_2](NO_3)_2(H_2O)_2$ (**2**), $[Cd(H_2O)_4(L_1)_2](NO_3)_2(H_2O)_2$ (**3**), $[Zn(L_1)(NO_3)(H_2O)_3](NO_3)$ (**4**), $[Cd(L_1)_2(NO_3)_2(H_2O)_2]$ (**5**, **6**), $[Cd_2(bdc)(L_1)_2(NO_3)_2(H_2O)_4]\cdot 2H_2O$ (**7**), $[Zn(H_2O)_4(L_2)_2](NO_3)_2$ (**8**), $[Cd(L_2)_2(NO_3)_2(H_2O)]$ (**9**), $[Zn(L_2)_2(CH_3COO)_2]$ (**10**), $[Cd(L_2)_2(CH_3COO)_2(Im)_{0.75}(H_2O)_{0.25}]\cdot 0.5(H_2O)$ (**11**), $[Zn(Cl)_2(L_1)(H_2O)]$ (**12**), $\{[Zn(Cl)_2(L_1)]\ 1/6(L_1\cdot H_2O)\}_n$ (**13**), and $[Cd(L_2)_6]_2[Cd(H_2O)_6](ClO_4)_6\cdot 7(H_2O)$ (**14**). Herein, for the first time, the Zn and Cd coordination compounds with L_1 and L_2 luminophores as inner-sphere ligands have been obtained and structurally characterized. The structural landscape includes inclusion compound **1**, supramolecular isomers **1**−**3**, isomorphs **2** and **3**, polymorphs **5** and **6**, and one-dimensional coordination polymer **13**. In discrete complexes, both luminophores coordinate to the metals in monodentate mode; in **13**, L_1 acts as a bidentate bridging ligand giving rise to the structure extension. Since the crystal packing and stacking patterns of the luminophore molecules are important factors underlying the aggregation induced emission, the finite and infinite stacking motifs registered in the crystal structures **1**−**14** are reported. All compounds reveal an emissive response upon irradiation under the UV−vis lamp. The best performing compounds in the series, namely, **4**, **5**, and **10**, have been fully spectroscopically characterized.

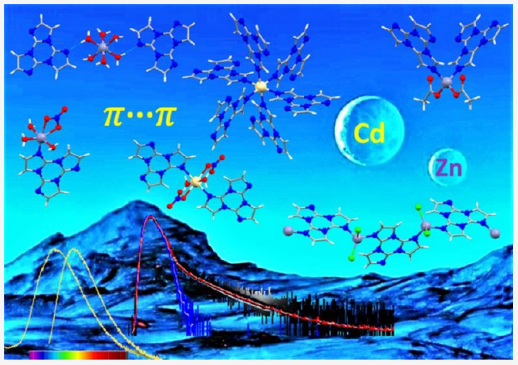

INTRODUCTION

In the past decade, substantial research has been focused on new energy-saving concepts for lighting and display applications. Organic light-emitting diodes (OLEDs) are promising devices for this task, since they consume only a fraction of the energy of conventional, inefficient light bulbs and can be manufactured on thin, flexible, and lightweight substrates. The concept of aggregation induced emission (AIE) pioneered by Tang et al. in 2001[1] nowadays is intensively studied for the above-mentioned applications.[2−4] Most of the AIE materials exhibit high fluorescence quantum yields (QY) in the solid state or in colloidal aggregates but weak fluorescence in dilute solutions. Among the factors responsible for the AIE phenomenon, the restriction of intramolecular rotation (RIR) and/or intramolecular motion (RIM), heavy-atom (halogen) effect, impact of hydrogen bonding, and favorable arrangement of luminophores in the crystal lattice[1−17] should be mentioned, all leading to a suppression of radiationless deactivation pathways.

The widespread research for a better understanding of the factors essential to optimizing emission properties in the solid state revealed that packing features are among the most important in affecting the bright fluorescence and room temperature phosphorescence (RTP).[2−4] In order to obtain ultralong phosphorescence (RTUP), a stable long-lived excited triplet state (T_1) is a necessary condition. It has been proven that the packing mode with strong $\pi-\pi$ interactions is one of the most effective features in stabilizing the T_1 state, resulting in persistent RTP.[6,18,19]

Although organic dyes exhibit broad emission wavelengths and tunability for optical gain materials, they are affected by poor optical and thermal stability. Amid the approaches to overcome such shortcomings, it has been proposed to load and isolate the dye molecules in the cavities of porous oxides and

Received: April 21, 2021
Revised: May 18, 2021

ACS Publications © XXXX American Chemical Society

metal−organic frameworks (MOFs)[20] or to build up discrete coordination compounds/coordination polymers with the luminophores as the ligands/linkers. The growing interest in the photochemistry and photophysics of Zn(II) and Cd(II) coordination compounds in the forms of discrete and polymeric species resulted in electroluminescent materials used in OLEDs.[21−25] Due to the high ionization potentials of these closed shell metal ions, 40 eV for Zn(II) and 38 eV for Cd(II), it is expected that excited states with a main D-metal contribution are located at high energy, while those with predominant ligand-centered and/or ligand−ligand charge transfer character should be at lower energy. Due to the d^{10} metals' flexible coordination numbers and stacking arrangements, a plethora of emissive behaviors is observed when a "purely" organic material is involved in the corresponding coordination compound.[21−25] The design of materials combining a highly emissive ligand and optically inactive metal ions, such as Zn(II) and Cd(II), allows tuning of the ligands' arrangements and, therefore, emissive properties such as lifetime, quantum yield, and stability of emitters. Furthermore, these materials compete with platinum group compounds in view of the metals' low cost and availability. Luminescent MOFs (LMOF) and coordination polymers (LCP) with tunable emissive behavior across the entire visible spectrum in addition to direct white light production have been reported.[24] Investigations on Zn/Cd carboxylic networks with impressive luminescence and highly tunable afterglow phosphorescence properties have been carried out including rationalization of the factors contributing to the emission efficacy (guest-induced effect, rigidification of coordination network, increase of luminophore population in the coordination network, parallel-displaced "J-type" aggregation molecular packing interactions of conjugate systems).[25−32] Besides aromatic carboxylic acids, the N-heterocyclic carbene (NHC) compounds[33] are other important luminescent ligands,[6,7,33−38] although organometallic light-emitting materials derived from poly-NHC ligands are still underdeveloped.[38] On the other hand, although many examples of Zn(II)/Cd(II) complexes with fast radiative decays have been reported, isolation of materials with longer lifetimes (τ > 0.1 s) remains more challenging,[39−41] and works in this field are still rare. For example, Yuan et al.[39] reported the compounds consisting of Zn(II) or Cd(II) and tri(4-imidazolylphenyl)amine, which exhibit long-persistent phosphorescence on a time scale up to seconds (ca. 2 s) at 77 K. Cepeda et al.[40] documented coordination polymer $[Zn(\mu\text{-}6ani)_2]_n$ (6ani = 6-aminonicotinic acid) that consists of stacked 2D neutral layers and displays a remarkably long-lasting green luminescence spanning out for about two seconds at room temperature, originated from the LMCT triplet state according to TD-DFT calculations.

The present study focuses on the preparation, structural characterization, and investigation of emission properties of Zn(II) and Cd(II) coordination compounds based on triimidazo[1,2-*a*:1′,2′-*c*:1″,2″-*e*][1,3,5]triazine (L_1) and its positional isomer, triimidazo[1,2-*a*:1′2′-*c*:1″,5″-*e*][1,3,5]-triazine (L_2) (Scheme 1).

L_1 is characterized by AIE behavior, comprising one fluorescence component at 425 nm and an ultralong phosphorescence (1 s) at 520 nm under ambient conditions (overall quantum efficiency equal to 30%), the latter associated with the presence of H-aggregates in the crystalline structure.[6] Its positional isomer, L_2, also revealed meaningful emissive properties in the solid state (λ_{max} = 415 nm, Φ = 13%),

Scheme 1. Molecular Structures of Triimidazo[1,2-*a*:1′,2′-*c*:1″,2″-*e*][1,3,5]triazine (L_1) and Its Positional Isomer, Triimidazo[1,2-*a*:1′2′-*c*:1″,5″-*e*][1,3,5]triazine (L_2)

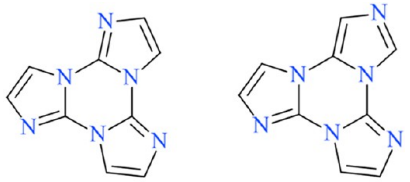

associated with fast deactivation channels (in the nanosecond region).[6] Furthermore, thanks to its nitrogen atoms available for coordination to metal atoms, L_1 has been successfully employed for the preparation of Cu(I) and Ag(I) coordination networks where L_1 behaves as a mono-, bi-, and tridentate ligand, giving rise to one-, two-, and three-dimensional (1D, 2D, 3D) coordination polymeric networks of different topologies.[34,42] Very recently, L_1 and L_2 ligands have been used for the synthesis of Cu(II) mononuclear and binuclear discrete complexes and 1D coordination polymers.[43] On the other hand, our first attempts to obtain Zn(II) or Cd(II) coordination compounds with an L_1 luminophore resulted in four inclusion compounds, where L_1 shows different aggregation stacking patterns, and the resulting compounds retain the emissive properties where the metal atom behaves as an external perturber.[35] In particular, in $[Zn_3(CH_3COO)_6(H_2O)_2](L_1)_2$, the luminophore molecules associate in a way very similar to the L_1 pure phase, but the increased spin−orbit coupling (SOC) manifests in an easier singlet-to-triplet intersystem crossing (ISC) resulting in intensification of the RTUP with respect to the fluorescence and in the appearance of the S_0-T^H transition in the excitation spectrum, T^H being the triplet state responsible for the phosphorescent emission. These results provided further contributions in the knowledge of RTUP from extrinsically perturbed organic materials in the solid state. Herein, for the first time, the Zn and Cd coordination compounds with L_1 and L_2 luminophores as inner-sphere ligands have been obtained and structurally characterized. Since the crystal packing and stacking patterns of the luminophore molecules are important for the AIE, the finite and infinite stacking motifs registered in the crystal structures of **1**−**14** are reported. All compounds reveal an emissive response upon irradiation under the UV−vis lamp. Due to the difficulties in obtaining batches of the compounds with the sufficient purity grade required to perform reliable photophysical studies and consequently derive congruent radiative deactivation mechanisms, photophysical characterization has been carried out for the three of them that revealed the strongest signals at the preliminary stages of the studies.

EXPERIMENTAL SECTION

Materials and Methods. All reagents and solvents were obtained from commercial sources and used without further purification. Ligands L_1 and L_2 were prepared according to literature procedures.[44,45]

General Synthetic Procedures. Solvothermal reactions for **1**, **2**, **4**−**8**, and **12**−**14** were performed using a sealed 12 mL Teflon-lined reactor, heated (0.41(6)°C/min rate) in an oven at 80 °C for 24 h, and slowly (0.023 °C/min rate) cooled to 30 °C. The reactions for **9**−**11** were carried out at 100 °C for 48 h following slow cooling. In typical reactions, the starting salt, L_1/L_2, was taken in a 1:1 molar

https://doi.org/10.1021/acs.cgd.1c00459
Cryst. Growth Des. XXXX, XXX, XXX−XXX

ratio; CH_3CN or CH_3CN/DMF solvent mixtures were taken in 7−10 mL amounts. After cooling, the reaction mixtures were filtered off and left for crystallization at room temperature. Elemental analysis (C, N, H) was performed on a Vario EL III Element Analyzer.

*Synthesis of $[Zn(H_2O)_6](NO_3)_2(L_1)_2$ (**1**) and $[Zn(H_2O)_4(L_1)_2](NO_3)_2(H_2O)_2$ (**2**).* In a Teflon beaker, in CH_3CN (10 mL), was added $Zn(NO_3)_2{\cdot}6H_2O$ (30.5 mg, 0.102 mmol) and L_1 (19.7 mg, 0.099 mmol). Transparent colorless plate-shaped crystals of **1** and block-shaped crystals of **2** were precipitated simultaneously in 4 days and separated manually. Yield for **1**: 20%. Elemental analysis, found (calcd), % for $C_{18}H_{24}N_{14}O_{12}Zn$: C, 31.16 (31.90); H, 3.49 (4.00); N, 28.26 (28.19). Yield for **2**: 25%. Elemental analysis, found (calcd), % for $C_{18}H_{24}N_{14}O_{12}Zn$: C, 31.16 (31.45); H, 3.49 (3.71); N, 28.26 (28.32).

*Synthesis of $[Cd(H_2O)_4(L_1)_2](NO_3)_2(H_2O)_2$ (**3**).* $Cd(NO_3)_2{\cdot}4H_2O$ was preliminarily dehydrated by heating to 190 °C, then cooled to room temperature. A mixture of $Cd(NO_3)_2$ (0.024 g, 0.1 mmol) and L_1 (0.02 g, 0.1 mmol) in CH_3CN (7 mL) was added in a Teflon-lined stainless steel autoclave, which was heated at 120 °C for 48 h. After the autoclave had been cooled at a rate of 18 °C for 1 h to 25 °C, colorless crystals of **3** were collected and dried in the air. Yield: 60%. Elemental analysis, found (calcd), % for $C_{18}H_{24}CdN_{14}O_{12}$: C, 29.18 (29.54); H, 3.26 (3.48); N, 26.47 (27.02).

*Synthesis of $[Zn(L_1)(NO_3)(H_2O)_3](NO_3)$ (**4**).* In a Teflon beaker, in CH_3CN (8 mL), was added $Zn(NO_3)_2{\cdot}6H_2O$ (30.5 mg, 0.102 mmol), L_1 (20.3 mg, 0.102 mmol), and H_2bdc (17.3 mg, 0.104 mmol). Transparent colorless crystals were precipitated in 2 weeks. Yield: 35%. Elemental analysis, found (calcd), % for $C_9H_{12}N_8O_9Zn$: C, 24.48 (24.96); H, 2.74 (3.08); N, 25.37 (25.73).

*Synthesis of $[Cd(L_1)_2(NO_3)_2(H_2O)_2]$ (**5**) and $[Cd_2(bdc)(L_1)_2(NO_3)_2(H_2O)_4]{\cdot}2H_2O$ (**7**).* In a Teflon beaker, in CH_3CN (8 mL), was added $Cd(NO_3)_2{\cdot}4H_2O$ (31.5 mg, 0.102 mmol), L_1 (22.4 mg, 0.113 mmol), and H_2bdc (17.5 mg, 0.105 mmol). Transparent colorless prism-shaped crystals of **5** were precipitated in 3 weeks. Yield: 50%. Elemental analysis, found (calcd), % for $C_{18}H_{16}CdN_{14}O_8$: C, 32.32 (32.54); H, 2.41 (2.58); N, 29.32 (28.90). Thin needles of **7** were coprecipitated and separated manually. Yield: 12%. Elemental analysis, found (calcd), % for $C_{26}H_{28}Cd_2N_{14}O_{16}$: C, 30.69 (31.12); H, 2.77 (2.22); N, 19.27 (19.64).

*Synthesis of $[Cd(L_1)_2(NO_3)_2(H_2O)_2]$ (**6**).* In a Teflon beaker, in CH_3CN (8 mL) was added $Cd(NO_3)_2{\cdot}4H_2O$ (36 mg, 0.116 mmol) and L_1 (21 mg, 0.106 mmol). Transparent colorless plate-shaped crystals were precipitated in 3 weeks. Yield: 43%. Elemental analysis, found (calcd), % for $C_{18}H_{16}CdN_{14}O_8$ C, 32.32 (32.60); H, 2.41 (2.04); N, 29.32 (28.69).

*Synthesis of $[Zn(H_2O)_4(L_2)_2](NO_3)_2$ (**8**).* In a Teflon beaker, in CH_3CN (8 mL), was added $Zn(NO_3)_2{\cdot}6H_2O$ (35 mg, 0.117 mmol) and L_2 (24 mg, 0.121 mmol). Transparent colorless crystals were precipitated in 3 weeks. Yield: 55%. Elemental analysis, found (calcd), % for $C_{18}H_{20}N_{14}O_{10}Zn$: C, 32.86 (32.24); H, 3.06 (2.85); N, 29.81 (29.19).

*Synthesis of $[Cd(NO_3)_2(H_2O)(L_2)_2]$ (**9**).* In a Teflon beaker, in CH_3CN (7 mL) and DMF (1 mL), was added $Cd(NO_3)_2{\cdot}4H_2O$ (32 mg, 0.103 mmol) and L_2 (20.1 mg, 0.101 mmol). Transparent colorless crystals were precipitated in 1 month. Yield: 45%. Elemental analysis, found (calcd), % for $C_{18}H_{14}CdN_{14}O_7$: C, 33.22 (33.87); H, 2.17 (2.54); N, 30.13 (29.18).

*Synthesis of $[Zn(L_2)_2(Ac)_2]$ (**10**).* In a Teflon beaker, in CH_3CN (7 mL) and DMF (1 mL), was added $Zn(CH_3COO)_2{\cdot}2H_2O$ (21 mg, 0.095 mmol) and L_2 (20 mg, 0.101 mmol). Transparent colorless crystals were precipitated in 1 month. Yield: 60%. Elemental analysis, found (calcd), % for $C_{22}H_{18}N_{12}O_4Zn$: C, 45.57 (45.12); H, 3.13 (2.88); N, 28.99 (28.24).

*Synthesis of $[Cd(L_2)_2(Ac)_2(Im)_{0.75}(H_2O)_{0.25}]{\cdot}0.5(H_2O)$ (**11**).* In a Teflon beaker, in CH_3CN (7 mL) and DMF (1 mL), was added $Cd(CH_3COO)_2{\cdot}2H_2O$ (24 mg, 0.09 mmol) and L_2 (20 mg, 0.101 mmol). Transparent colorless crystals were precipitated in 2 weeks. Yield: 35%. Elemental analysis, found (calcd), % for $C_{24.25}H_{21.75}CdN_{13.5}O_{4.75}$: C, 42.17 (42.54); H, 3.17 (3.85); N, 27.38 (26.83).

*Synthesis of $[Zn(Cl)_2(L_1)(H_2O)]$ (**12**) and $\{[Zn(Cl)_2(L_1)]{\cdot}1/6(L_1){\cdot}1/6(H_2O)\}_n$ (**13**).* In a Teflon beaker, in CH_3CN (8 mL), was added $ZnCl_2$ (14.3 mg, 0.104 mmol), L_1 (21.6 mg, 0.109 mmol), and H_2bdc (17.2 mg, 0.103 mmol). Transparent colorless block-shaped crystals of **12** were precipitated in 4 days. Yield: 30%. Elemental analysis, found (calcd), % for $C_9H_8Cl_2N_6OZn$: C, 30.67 (29.39); H, 2.29 (2.01); N, 23.84 (23.15). After 3 weeks, needle crystals of **13** were precipitated. Yield: 18%. Elemental analysis, found (calcd), % for $C_{10.5}H_{7.33}Cl_2N_7O_{0.17}Zn$: C, 34.04 (33.40); H, 1.99 (2.30); N, 26.46 (25.99).

*Synthesis of $[Cd(L_2)_6]_2[Cd(H_2O)_6](ClO_4)_6$ 7(H_2O) (**14**).* In a Teflon beaker, in CH_3CN (8 mL), was added $Cd(ClO_4)_2{\cdot}xH_2O$ (34.9 mg, 0.112 mmol), L_2 (24 mg, 0.121 mmol), and H_2bdc (17.4 mg, 0.104 mmol). Transparent colorless crystals were precipitated in 2 weeks. Yield: 55%. Elemental analysis, found (calcd), % for $C_{36}H_{32}CdCl_2N_{24}O_{12.52}$: C, 36.58 (36.11); H, 2.73 (2.12); N, 28.44 (28.02).

Crystallographic Studies. Diffraction measurements for **1**−**14** were carried out on an Xcalibur E diffractometer equipped with a CCD area detector and a graphite monochromator utilizing Mo Kα radiation at a room temperature. Final unit cell dimensions were obtained and refined on an entire data set. All calculations to solve the structures and to refine the models proposed were carried out with the programs SHELXS97 and SHELXL2014.[46,47] In compound **6**, oxygen atoms in one nitrate anion are disordered over two positions and refined with the partial occupancies 0.628(5):0.372(5). Compound **9** was refined as a two-component twin. In compound **11**, the coordinated imidazole molecule that resides on a 2-fold axis alternates in this position with coordinated and outer-sphere water molecules, the components were refined with a 0.75:0.25 population ratio. Compound **12** was refined as an inversion twin with the ratio of components 0.514:0.486. The structure is completely disordered; each formula unit is disordered over two positions, with occupancies 0.822(17):0.178(17) and 0.679(19):0.321(19), respectively. In **13**, the outer-sphere L_1 and water molecules are disordered over a 3-fold axis and refined with incomplete occupancies. Hydrogen atoms attached to carbon atoms were positioned geometrically and treated as riding atoms using SHELXL default parameters with $U_{iso}(H) = 1.2U_{eq}(C)$ and $U_{iso}(H) = 1.5U_{eq}(C,O)$ for methyl groups and water molecules. In water molecules with full occupancies, H atoms were found at the preliminary stages of the refinement and finally refined in fixed positions. In crystal structure **14**, H atoms in the partly populated outer-sphere water molecules were not localized. The X-ray data and the details of the refinement for **1**−**4** are summarized in Table 1. The figures were produced using MERCURY software.[48] Calculations of $\pi\cdots\pi$ stacking parameters (Cg···Cg distances, interplanar angles) were performed using PLATON software.[49] The geometric parameters are given in CIF files. CIF files were deposited with the CSD, deposition numbers CCDC 2076858−2076871.

RESULTS AND DISCUSSION

Solvothermal reactions using blends of Zn(II)/Cd(II) salts, $Zn(NO_3)_2{\cdot}6H_2O$, $Cd(NO_3)_2{\cdot}4H_2O$, $Zn(CH_3COO)_2{\cdot}2H_2O$, $Cd(CH_3COO)_2{\cdot}2H_2O$, $ZnCl_2{\cdot}2H_2O$, and $Cd(ClO_4)_2{\cdot}xH_2O$ with either L_1 or L_2 luminophores resulted in 14 new crystalline solids formulated as $[Zn(H_2O)_6](NO_3)_2(L_1)_2$ (**1**), $Zn(H_2O)_4(L_1)_2](NO_3)_2(H_2O)_2$ (**2**), $[Cd(H_2O)_4(L_1)_2](NO_3)_2(H_2O)_2$ (**3**), $[Zn(L_1)(NO_3)(H_2O)_3](NO_3)$ (**4**), $[Cd(L_1)_2(NO_3)_2(H_2O)_2]$ (**5**, **6**), $[Cd_2(bdc)(L_1)_2(NO_3)_2(H_2O)_4]{\cdot}2H_2O$ (bdc = 1,4-benzenedicarboxylate) (**7**), $[Zn(H_2O)_4(L_2)_2](NO_3)_2$ (**8**), $[Cd(L_2)_2(NO_3)_2(H_2O)]$ (**9**), $[Zn(L_2)_2(Ac)_2]$ (**10**), $[Cd(L_2)_2(Ac)_2(Im)_{0.75}(H_2O)_{0.25}]{\cdot}0.5(H_2O)$ (Im = imidazole) (**11**), $[Zn(Cl)_2(L_1)(H_2O)]$ (**12**), $(\{[Zn(Cl)_2(L_1)]{\cdot}1/6(L_1{\cdot}H_2O)\}_n$ (**13**), and $L_2)_6]_2[Cd(H_2O)_6](ClO_4)_6{\cdot}7(H_2O)$ (**14**), whose crystal structures were studied by single crystal X-ray diffraction structural analysis. The crystallographic data for **1**−**14** are summarized in Table 1. The bond distances and angles in the metals' coordination cores in

https://doi.org/10.1021/acs.cgd.1c00459
Cryst. Growth Des. XXXX, XXX, XXX−XXX

Table 1. Crystal Data and Structure Refinement Parameters for Compounds 1−7

	compound number						
	1	**2**	**3**	**4**	**5**	**6**	**7**
composition	$[Zn(H_2O)_6](NO_3)_2(L_1)_2$	$[Zn(H_2O)_4(L_1)_2](NO_3)_2(H_2O)_2$	$[Cd(H_2O)_4(L_1)_2](NO_3)_2(H_2O)_2$	$[Zn(L_1)(NO_3)(H_2O)_3](NO_3)$	$[Cd(L_1)_2(NO_3)_2(H_2O)_2]$	$[Cd(L_1)_2(NO_3)_2(H_2O)_2]$	$[Cd_2(bdc)(L_1)_2(NO_3)_2(H_2O)_4]\cdot 2H_2O$
empirical formula	$C_{18}H_{24}N_{14}O_{12}Zn$	$C_{18}H_{24}N_{14}O_{12}Zn$	$C_{18}H_{24}CdN_{14}O_{12}$	$C_9H_{12}N_8O_9Zn$	$C_{18}H_{16}CdN_{14}O_8$	$C_{18}H_{16}CdN_{14}O_8$	$C_{26}H_{28}Cd_2N_{14}O_{16}$
formula weight	693.88	693.88	740.91	441.64	668.85	668.85	1017.42
crystal system	triclinic	triclinic	triclinic	triclinic	monoclinic	monoclinic	monoclinic
space group	$P\bar{1}$	$P\bar{1}$	$P\bar{1}$	$P\bar{1}$	$C2/c$	$P2_1/n$	$P2_1/n$
a, Å	8.0765(6)	7.1668(8)	7.2358(10)	8.5471(7)	25.8206(13)	7.2334(2)	8.8497(4)
b, Å	9.1056(7)	8.2481(9)	8.2970(13)	9.1061(7)	6.9849(5)	14.0028(4)	19.3876(12)
c, Å	10.2014(8)	11.5772(14)	11.640(2)	11.1282(6)	13.5066(6)	22.4443(6)	10.3001(4)
α, deg	71.701(7)	89.759(10)	89.688(14)	85.539(5)	90	90	90
β, deg	76.625(7)	83.656(10)	83.904(13)	78.333(6).	101.938(5)	91.314(3)	95.210(4)
γ, deg	77.036(7)	73.406(10)	73.517(13)	66.208(8)	90	90	90
volume, Å^3	683.56(10)	651.57(14)	666.08(19)	776.13(10)	2383.3(2)	2272.74(11)	1759.94(15)
Z	1	1	1	2	4	4	2
D (calcd), mg/m^3	1.686	1.768	1.847	1.890	1.864	1.955	1.920
μ, mm^{-1}	0.987	1.035	0.911	1.654	0.995	1.044	1.304
$F(000)$	356	356	374	448	1336	1336	1012
index ranges	$-9 \le h \le 9$	$-8 \le h \le 8$	$-8 \le h \le 7$	$-10 \le h \le 10$	$-21 \le h \le 31$	$-8 \le h \le 8$	$-10 \le h \le 10$
	$-11 \le k \le 8$	$-6 \le k \le 9$	$-10 \le k \le 9$	$-10 \le k \le 10$	$-8 \le k \le 4$	$-16 \le k \le 16$	$-23 \le k \le 12$
	$-11 \le l \le 12$	$-14 \le l \le 13$	$-14 \le l \le 13$	$-13 \le l \le 12$	$-16 \le l \le 13$	$-27 \le l \le 17$	$-12 \le l \le 8$
reflections collected	3767	3599	4121	4895	4302	8886	6238
independent reflections	2519 [R_{int} = 0.0240]	2403 [R_{int} = 0.0220]	2476 [R_{int} = 0.0539]	2800 [R_{int} = 0.0236]	2226 [R_{int} = 0.0275]	4195 [R_{int} = 0.0250]	3277 [R_{int} = 0.0436]
data/restraints/parameters	2519/9/229	2403/9/230	2476/12/229	2800/0/254	2226/3/196	4195/42/415	3277/10/280
goodness-of-fit on F^2	1.071	1.063	1.086	1.088	1.051	1.005	0.956
final R indices [$I > 2\sigma(I)$], R_1, wR_2	0.0440, 0.0932	0.0370, 0.0824	0.0625, 0.1546	0.0366, 0.0785	0.0347, 0.0885	0.0309, 0.0674	0.0534, 0.0721
R indices all data), R_1,wR_2	0.0567, 0.1018	0.0438, 0.0870	0.0666, 0.1584	0.0428, 0.0830	0.0425, 0.0954	0.0390, 0.0710	0.0933, 0.0850

	compound number						
	8	**9**	**10**	**11**	**12**	**13**	**14**
composition	$[Zn(H_2O)_4(L_2)_2](NO_3)_2$	$[Cd(NO_3)_2(H_2O)(L_2)_2]$	$[Zn(L_2)_2(Ac)_2]$	$[Cd(L_2)_2(Ac)_2(Im)_{0.75}(H_2O)_{0.25}]\cdot 0.5(H_2O)$	$[Zn(Cl)_2(L_1)(H_2O)]$	$\{[Zn(Cl)_2(L_1)]\cdot 1/6(L_1)\cdot 1/6(H_2O)\}_n$	$[Cd(L_2)_6]_2[Cd(H_2O)_6](ClO_4)_6$ 7(H_2O)
empirical formula	$C_{18}H_{20}N_{14}O_{10}Zn$	$C_{18}H_{14}CdN_{14}O_7$	$C_{22}H_{18}N_{12}O_4Zn$	$C_{24.25}H_{21.75}CdN_{13.5}O_{4.75}$	$C_9H_8Cl_2N_6OZn$	$C_{10.5}H_{7.33}Cl_2N_7O_{0.17}Zn$	$C_{108}H_{96}Cd_3Cl_6N_{72}O_{37.56}$
formula weight	657.85	650.83	579.85	690.70	352.48	370.50	3546.48
crystal system	monoclinic	triclinic	monoclinic	monoclinic	orthorhombic	trigonal	trigonal
space group	$P2_1/n$	$P\bar{1}$	$I2/c$	$C2/c$	$Pca2_1$	$R3c$	$R\bar{3}$
a, Å	11.6840(5)	6.8606(5)	18.5940(11)	23.0475(7)	13.5411(8)	24.956(3)	20.5390(12)
b, Å	9.5119(3)	10.4828(11)	5.8071(5)	8.4765(3)	16.3420(16)	24.956(3)	20.5390(12)
c, Å	12.6066(5)	16.851(2)	23.117(2)	14.1559(5)	11.8542(8)	12.8686(13)	29.7452(13)
α, deg	90	99.422(9)	90	90	90	90	90
β, deg	116.602(5)	100.783(8)	110.065(8)	100.117(3)	90	90	90
γ, deg	90	100.592(8)	90	90	90	120	120
volume, Å^3	1252.74(10)	1145.3(2)	2344.6(3)	2722.6(2)	2623.2(4)	6941(2)	10866.9(14)
Z	2	2	4	4	8	18	3

https://doi.org/10.1021/acs.cgd.1c00459
Cryst. Growth Des. XXXX, XXX, XXX−XXX

Table 1. continued

	compound number							
	8	9	10	11	12	13	14	
D (calcd), mg/m^3	1.744	1.887	1.643	1.685	1.785	1.596	1.626	
μ, mm^{-1}	1.066	1.030	1.107	0.866	2.280	1.941	0.649	
F(000)	672	648	1184	1391	1408	3324	5376	
index ranges	$-14\ h \le 14$	$-7\ h \le 8$	$-22\ h \le 15$	$-27\ h \le 25$	$-16\ h \le 11$	$-20\ h \le 29$	$-24\ h \le 20$	
	$-10 \le k \le 11$	$-12 \le k \le 12$	$-7\ k \le 6$	$-10\ k \le 9$	$-11\ k \le 19$	$-16\ k \le 26$	$-22\ k \le 20$	
	$-15 \le l \le 10$	$-20\ l \le 20$	$-19\ l \le 28$	$-16\ l \le 16$	$-14\ l \le 8$	$-10\ l \le 15$	$-25\ l \le 35$	
reflections collected	4269	7865	4109	4870	6625	4517	7426	
independent reflections	2338 [R_{int} = 0.0213]	7865	2162 [R_{int} = 0.0350]	2433 [R_{int} = 0.0236]	3501 [R_{int} = 0.0497]	1951 [R_{int} = 0.0678]	4494 [R_{int} = 0.0532]	
data/restraints/parameters	2338/6/209	7865/3/368	2162/0/178	2433/0/210	3501/149/506	1951/41/211	4494/15/355	
goodness-of-fit on F^2	1.088	0.959	1.006	1.004	1.001	1.004	0.998	
final R indices [$I > 2\sigma(I)$], R_1, wR_2	0.0397, 0.0981	0.0523, 0.1288	0.0450, 0.1040	0.0372, 0.1173	0.0567, 0.1161	0.0622, 0.1484	0.0666, 0.1448	
R indices all data), R_1,wR_2	0.0508, 0.1096	0.0728, 0.1357	0.0619, 0.1137	0.0472, 0.1242	0.0914, 0.1321	0.0870, 0.1648	0.1167, 0.1718	

1−**14** do not differ from the literature values[50] and are summarized in Table S1 and in the deposited CIF files. The hydrogen-bonding geometries are given in Table S2.

Crystal Structures and Supramolecular Architectures. The most populated group of complexes is that obtained from the blends of Zn(II)/Cd(II) nitrates, $Zn(NO_3)_2{\cdot}6H_2O$/$Cd(NO_3)_2{\cdot}4H_2O$ with L_1/L_2 luminophores, that includes eight mononuclear and one binuclear compound, $[Zn(H_2O)_6](NO_3)_2(L_1)_2$ (**1**), $[Zn(H_2O)_4(L_1)_2](NO_3)_2(H_2O)_2$ (**2**), $[Cd(H_2O)_4(L_1)_2](NO_3)_2(H_2O)_2$ (**3**), $[Zn(L_1)(NO_3)(H_2O)_3](NO_3)$ (**4**), $[Cd(L_1)_2(NO_3)_2(H_2O)_2]$ (**5**, **6**), $[Cd_2(bdc)(L_1)_2(NO_3)_2(H_2O)_4]{\cdot}2H_2O$ (bdc = 1,4-benzenedicarboxylate; **7**), $[Zn(H_2O)_4(L_2)_2](NO_3)_2$ (**8**), and $[Cd(L_2)_2(NO_3)_2(H_2O)]$ (**9**). The binuclear complex **7** was obtained as a coprecipitation product in the synthesis of **5** and is the only compound where the H_2bdc ligand used in the synthesis (see Experimental Section) was disclosed in the final crystalline product.

The structural diversity among complexes is originated from the water−anion−luminophore (L_1/L_2) interplay. The formula units for L_1-based mononuclear complexes **1**−**6** are depicted in Figure 1. The metal atoms reside on inversion centers in **1**−**3** and **5**, and in general positions in **4** and **6**, thus reflecting the asymmetry of the latter. The two L_1 ligands occupy opposite trans positions in metals' coordination cores and are situated in parallel planes in **2**, **3**, and **5** giving rise to extended L_1−M−L_1 platforms 17.076−17.592 Å long, as measured by the distance between the most distal H atoms. The L_1 ligand coordinates in a monodentate mode, leaving two other N atoms available for participation in hydrogen bonding interactions. In **4**, the Zn(II) equatorial platform is complimented by a chelate nitrate anion twisted at 18.1(2)° from the L_1 mean plane; in **6**, two L_1-wings form an interplanar angle of 52.26(3)°. Ionic compounds comprise complex cations $[Zn(H_2O)_6]^{2+}$ (**1**), $[Zn(H_2O)_4(L_1)_2]^{2+}$ (**2**), $[Cd(H_2O)_4(L_1)_2]^{2+}$ (**3**), and $[Zn(L_1)(NO_3)(H_2O)_3]^{+}$ (**4**) and outer-sphere nitrate-anions. The neutrality of $[Cd(L_1)_2(NO_3)_2(H_2O)_2]$ (**5**, **6**) polymorphs is reached by coordination of nitrate anions to Cd(II) atoms either in a monodentate mode as in **5** or in monodentate and bidentate chelate modes as in **6**.[51] The Zn(II) atoms take the octahedral coordination geometry, O_6 being the ideal one in **1** and the N_2O_4 or NO_5 distorted ones in **3** and **4**, respectively. The Cd(II) atoms take either the N_2O_4 distorted octahedral (**3**, **5**) or the N_2O_5 pentagonal-bipyramidal (**6**) coordination geometries.

Water-rich compounds $[Zn(H_2O)_6](NO_3)_2(L_1)_2$ (**1**), $[Zn(H_2O)_4(L_1)_2](NO_3)_2(H_2O)_2$ (**2**), and $[Cd(H_2O)_4(L_1)_2](NO_3)_2(H_2O)_2$ (**3**) reveal the same ratio of components, crystallize in the same triclinic $P\bar{1}$ space group with comparable unit cell dimensions (Table 1) and represent supramolecular isomers, compounds **2** and **3** being isomorphous. The multiple water molecules, acting as powerful H donors, are responsible for the crucial impact of hydrogen bonds in crystal packing. **1** is actually a precursor of coordination complex, being an inclusion compound with L_1 accommodated as a guest in the crystal lattice. Each $[Zn(H_2O)_6]^{2+}$ cation is H-bonded with six L_1 luminophores situated in two parallel planes, and each L_1 molecule is linked with three adjacent $[Zn(H_2O)_6]^{2+}$ cations giving rise to supramolecular H-bonded double-layer motif parallel to the (111) plane and stabilized by six unique OH···N hydrogen bonds (Figure 2a). Remarkably, the OH(H_2O)···N(L_1) hydrogen bonds inside the supramolecular layer are shorter (2.755(3)−2.786(3) Å) than OH(H_2O)···O(NO_3^-)

https://doi.org/10.1021/acs.cgd.1c00459
Cryst. Growth Des. XXXX, XXX, XXX−XXX

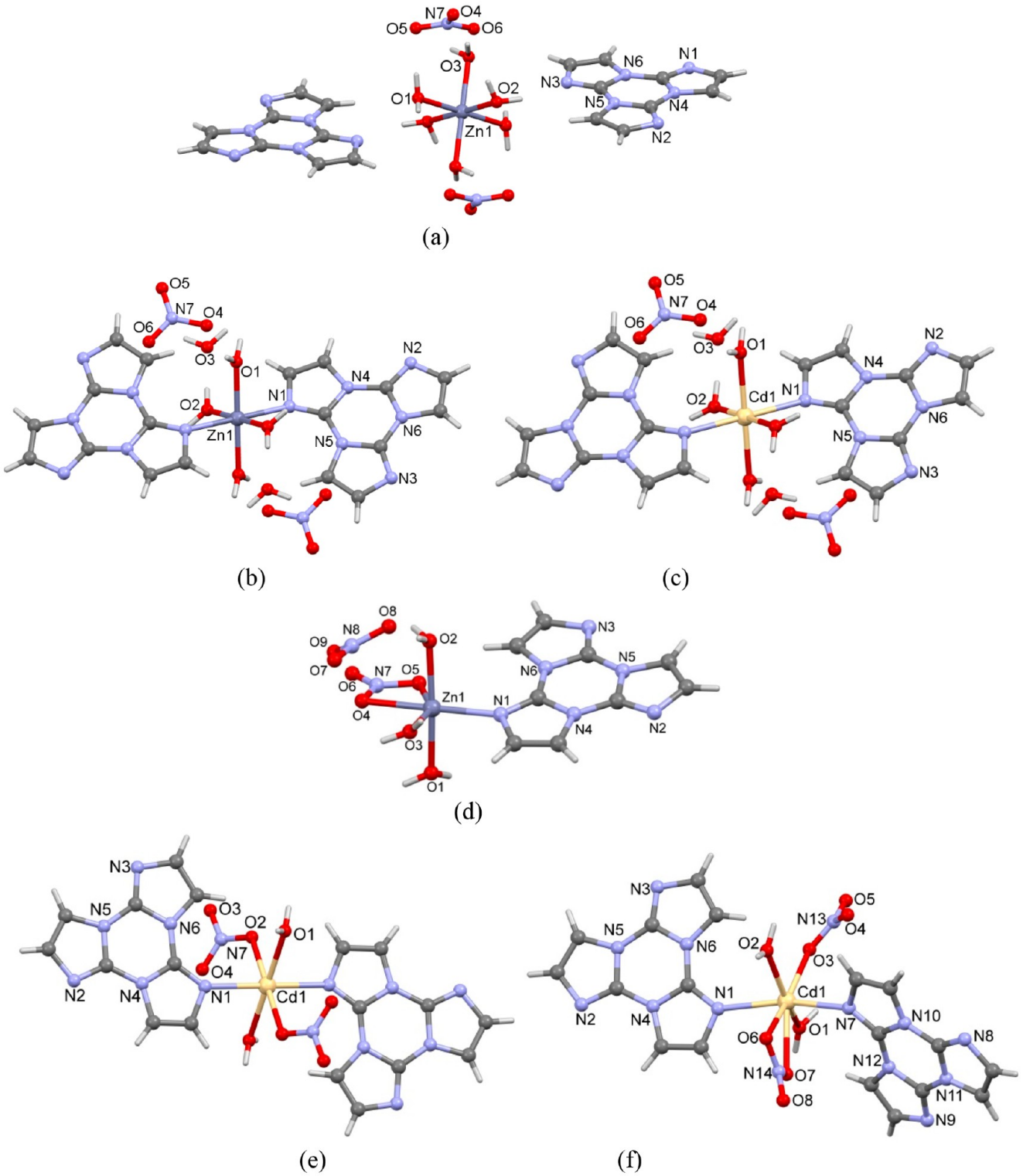

Figure 1. Views of formula units in **1**–**6** (a–f).

hydrogen bonds (2.831(3)–2.847(3) Å, Table S2) with participation of nitrate anions anchored to both surfaces of the layer (Figure 2b). This provides an L_1 assembling in centrosymmetric stacking dimers in the crystal. Evidently, complex $[Zn(H_2O)_6](NO_3)_2(L_1)_2$ (**1**) enriches the family of recently reported inclusion compounds $[M(H_2O)_6](An)_2(L_1)_2$ (M = Zn, Cd, An = BF_4^-, ClO_4^-)[35] with dissimilarities provoked by the different anions' geometries, being trigonal planar for the nitrate anion versus tetrahedral for tetrafluoroborate and perchlorate anions. In particular, L_1 molecules in **1** are placed in a slipped parallel mode in the stacking dimer (Figure S1a). The overlapping area includes the fused triazine (Tr) and imidazole (Im) rings, with an interplanar separation of 3.2522(12) Å and Cg(Tr)···Cg(Tr) (1 − *x*, 2 − *y*, −*z*) =

https://doi.org/10.1021/acs.cgd.1c00459
Cryst. Growth Des. XXXX, XXX, XXX−XXX

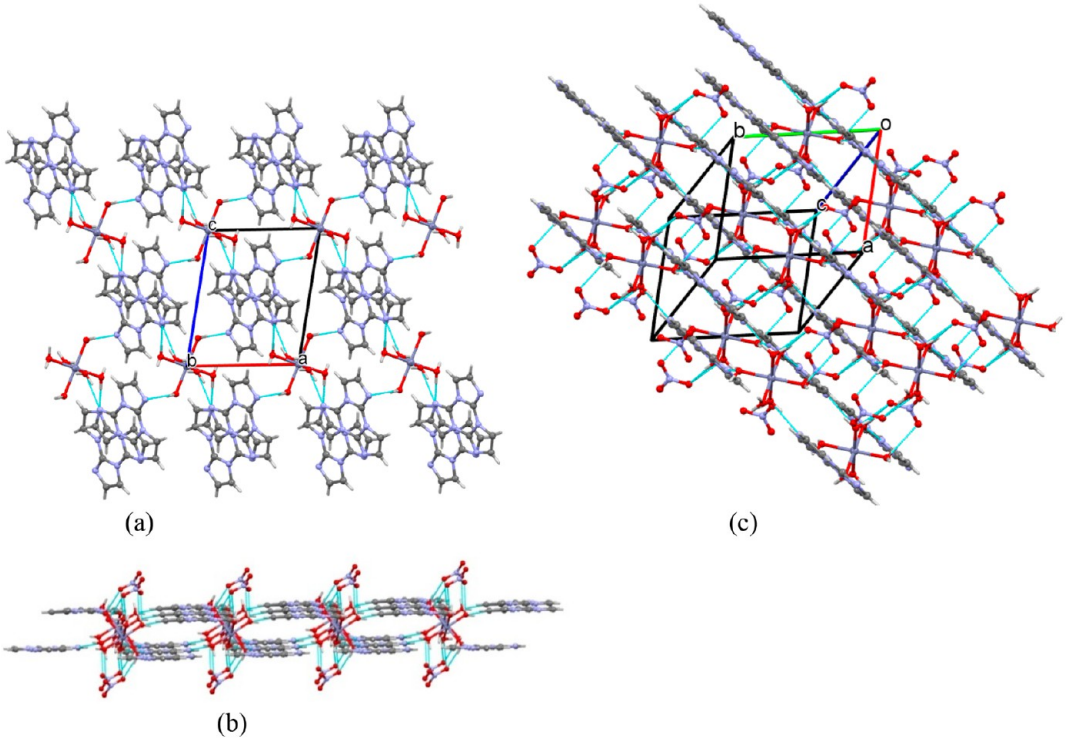

Figure 2. Crystal structure of compound **1**. (a) Association of $[Zn(H_2O)_6]^{2+}$ cations and L_1 in H-bonded layer, top view; (b) side view of cationic double layer with perching nitrate anions; (c) crystal packing with parallel arrangement of L_1.

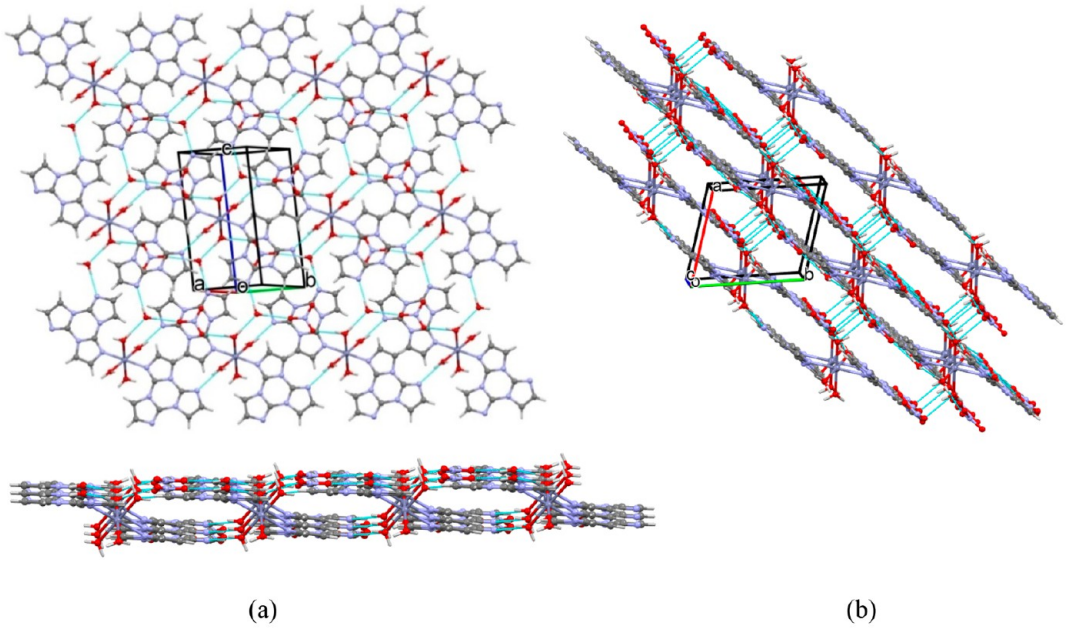

Figure 3. Crystal structure of compound **2**. (a) Association of components in supramolecular H-bonded double layer, top and side views; (b) crystal packing, with indication of H bonds between supramolecular layers.

3.5344(16) Å, against shorter Cg(Tr)···Cg(Tr) distances of 3.450 Å (for M = Cd; An = ClO_4^-) and 3.423 Å (M = Cd, Zn; An = BF_4^-) in the previously reported compounds where the triazine cycles overlap perfectly (Figure S1b). However, in all cases, the luminophore's possibilities for further aggregation are blocked by the perching anions. The observed dissimilarities in crystal structures reflect crystallization in different space groups, $P\bar{1}$ for **1** and $R\bar{3}$ for all three other compounds.[35]

The isomorphous compounds $[Zn(H_2O)_4(L_1)_2](NO_3)_2(H_2O)_2$ (**2**) and $[Cd(H_2O)_4(L_1)_2](NO_3)_2(H_2O)_2$ (**3**) reveal the replacement of two coordinated water molecules by two L_1 ligands that resulted in extended L_1−M−L_1 platforms, rigidified by M−N coordination bonds that substitute a pair of $OH(H_2O)\cdots N(L_1)$ hydrogen bonds registered in **1**. However, some crystal packing features are preserved. The supramolecular H-bonded double layer motif (Figure 3) now

https://doi.org/10.1021/acs.cgd.1c00459
Cryst. Growth Des. XXXX, XXX, XXX−XXX

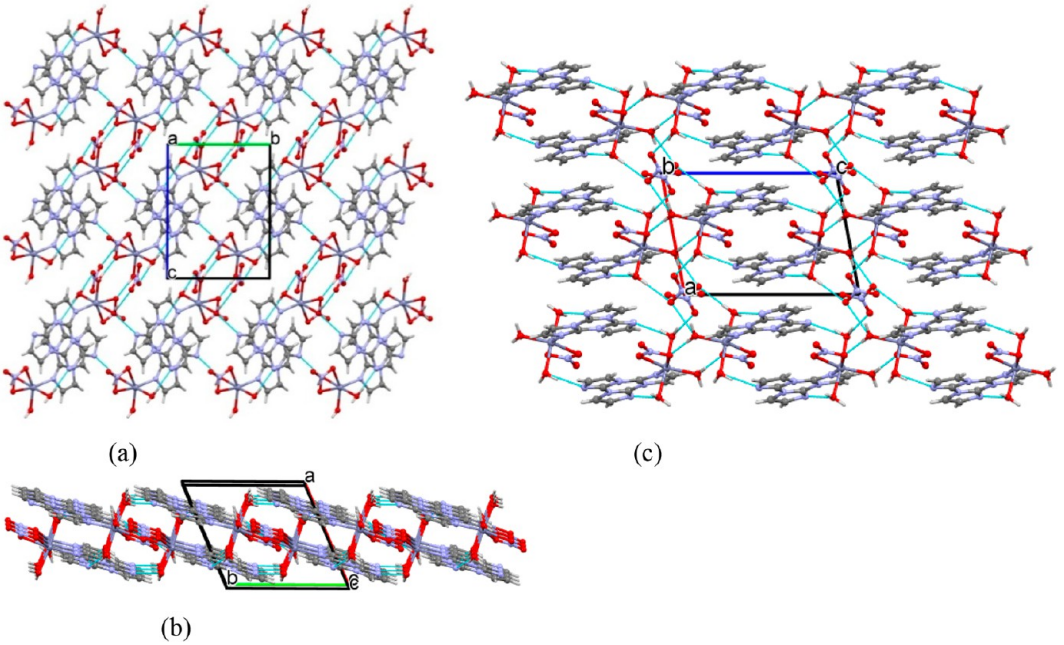

Figure 4. Crystal structure of compound **4**. (a) Fragment of crystal packing along the crystallographic *a* axis showing the stabilizing $H_2O\cdots NO_3^-$ and $OH(H_2O)\cdots N(L_1)$ hydrogen bonds; (b) side view of supramolecular cationic layer; (c) crystal packing showing L_1 stacking motif assisted by hydrogen bonds.

includes $[M(H_2O)_4(L_1)_2]^{2+}$ complex cations, outer-sphere nitrate anions, and water molecules, all species held together in a supramolecular layer that is situated parallel to the (110) plane (of six unique hydrogen bonds five are realized inside this layer, and only one is orthogonal to the layer). The nitrate anion, being linked with the inner-sphere water molecule *via* the $OH(H_2O)\cdots O(NO_3)$ hydrogen bond (Table S2), is situated roughly parallel to L_1, as indicated by the dihedral angle between their mean planes, 6.09(16)°. The nitrate anion and outer sphere water molecule perching above/below L_1 from the adjacent level (Figure 3) block any possible homomeric stacking pattern, replaced by the heteromeric water$\cdots L_1\cdots NO_3^-$ one (Figure S1c). Similarly to **1**, the arrangement is strongly influenced by H bonds inside the layer that are shorter and more numerous than the single one, $O(3)(H_2O)\cdots O(6)(NO_3^-)$, between the supramolecular layers (Table S2).

In the ionic crystal $[Zn(L_1)(NO_3)(H_2O)_3](NO_3)$ (**4**), self-association of complex cations $[Zn(L_1)(NO_3)(H_2O)_3]^+$ occurs parallel to the *bc* plane *via* a pair of $OH(H_2O)\cdots O(NO_3^-)$ hydrogen bonds in the form of the centrosymmetric supramolecular $R_2^2(8)$ synthon[52] giving rise to a centrosymmetric cationic dimer 22.68-Å-long. The association of these dimers *via* two $OH(H_2O)\cdots$N2/N3 (N2 and N3 being the L_1 noncoordinated nitrogen atoms) hydrogen bonds (Figure 4a, Table 1) results in a supramolecular cationic double layer with L_1 situated in parallel planes without overlap. Along the crystallographic *a* axis, the outer-sphere nitrate anions anchor to both surfaces of each cationic layer and bridge them *via* one single and one bifurcated $OH(H_2O)\cdots O(NO_3^-)$ hydrogen bond (Table S2) forming a 3D H-bonded network. This results in the formation of columns of coordinated L_1 luminophores along the *a* axis with alternating short and long separations between luminophores in columns. Similarly to **1**, a meaningful stacking interaction is established within the centrosymmetric dimer with similar a Tr−Im contour, having an interplanar separation of 3.3209(12) Å and Cg(Tr)$\cdots$Cg(Tr) ($-x$, $-y$, $1-z$) distance of 3.8545(19) Å, alternating with Cg(Tr)$\cdots$Cg(Tr) ($1-x$, $-y$, $1-z$) distance equal to 5.1049(19) Å and an interplanar separation of 3.3815(12) Å (Figure S1d). Thus, the L_1 ligands form infinite stacking columns, and an additional, in comparison with the L_1 pure form, chromophores' planarization in the system is achieved *via* coordination and hydrogen bond interactions.

The neutral complex $[Cd(L_1)_2(NO_3)_2(H_2O)_2]$ was prepared in different synthetic conditions (Experimental Section) as two monoclinic polymorphs (Table 1), namely as prismatic crystals **5** (sp. gr. $C2/c$) and plate crystals **6** (sp. gr. $P2_1/n$). Complexes differ by molecular symmetries (C_i vs C_1, Figure 1e,f) and show both similarities and dissimilarities in crystal packings. In both structures, ligands in the Cd(II) equatorial planes (H_2O and NO_3^-) are linked *via* $OH(H_2O)\cdots O(NO_3^-)$ hydrogen bonds (Table S2) resulting in infinite supramolecular 2D H-bonding motifs parallel to the *bc* plane in **5** and *ab* plane in **6** (Figure 5a,b) with L_1 pillars lying orthogonally to these layers. Sufficient separation between adjacent pillars allows L_1 interdigitation along the crystallographic *a* axis in **5** and the *c* axis in **6** (Figure 5c,d), with the formation of stacking columns. In both polymorphs, $CH(L_1)\cdots N(L_1)$ edge-to-edge contacts, absent in **1**−**4** (Table S2) and typical for the L_1 pure form,[6] were registered. These homomeric side contacts are realized as either a centrosymmetric $R_2^2(10)$ homosynthon in **5** or acentric (generated by the 2-fold axis) $R_2^2(8)$ homosynthon in **6** (Figure S2a,b). In both structures, these contacts join adjacent stacking columns forming stacking layers with different degrees of corrugation (Figure 5e,f). The CH$\cdots$N side contacts complement the coordination and OH$\cdots$O hydrogen bonds and contribute to the luminophores' alignments in the crystals. In **5**, the alternating interplanar separations between antiparallel L_1 along the columns are 3.4376(11) and 3.3744(11) Å, with distances between centroids of triazine moieties alternately equal to Cg(Tr)$\cdots$

https://doi.org/10.1021/acs.cgd.1c00459
Cryst. Growth Des. XXXX, XXX, XXX−XXX

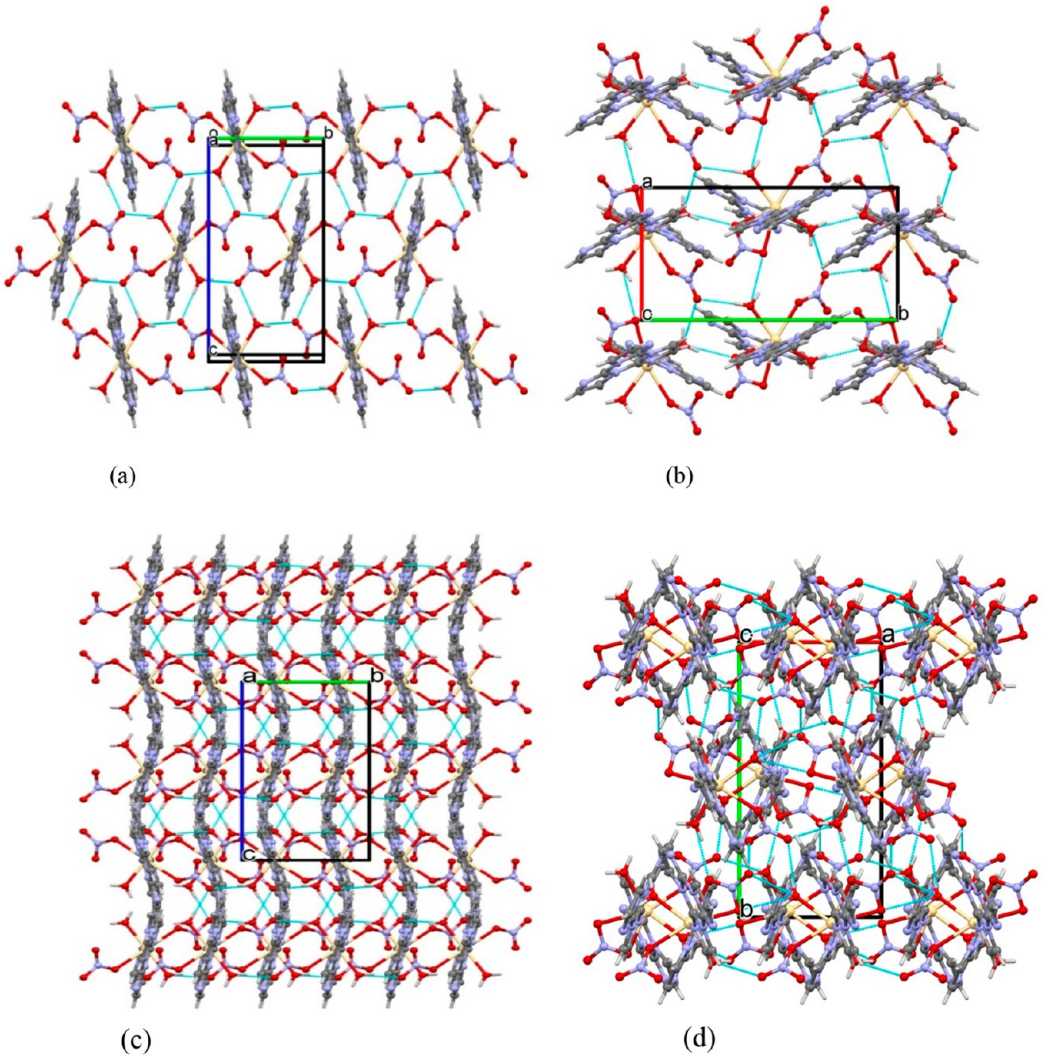

Figure 5. Fragments of crystal structures in polymorphs **5** and **6**. (a) Fragment of crystal packing in **5** showing the $OH(H_2O)\cdots O(NO_3^-)$ hydrogen bonds and L_1 pillars attached to supramolecular H-bonded inorganic layer; (b) the same in **6**; (c) view of stacking layer in **5**; (d) the same in **6**.

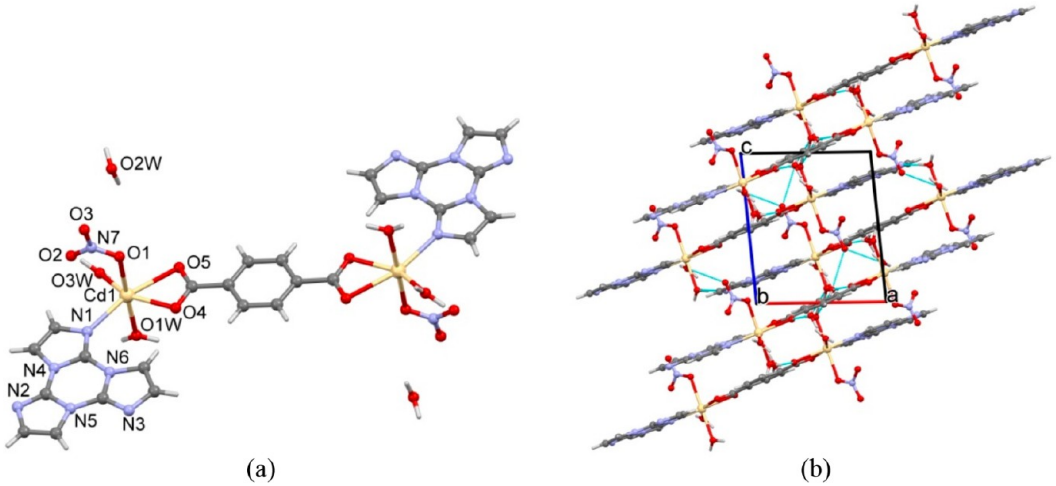

Figure 6. Crystal structure of compound **7**. (a) View of formula unit; (b) fragment of crystal packing showing stacking motifs and hydrogen bonds.

Cg(Tr) $(-x, -y, -z)$ = 4.8835(18) Å and Cg(Tr)···Cg(Tr) $(-x, 1 - y, -z)$ = 4.9379(17) Å (Figure S1e). Less homogeneous Cg···Cg separations are found along the columns of ligands in **6** due to the complex's asymmetry. In the columns, partially overlapping stacking dimers alternate. Separations within alternating dimers are Cg(Tr1)···Cg(Tr1)

https://doi.org/10.1021/acs.cgd.1c00459
Cryst. Growth Des. XXXX, XXX, XXX−XXX

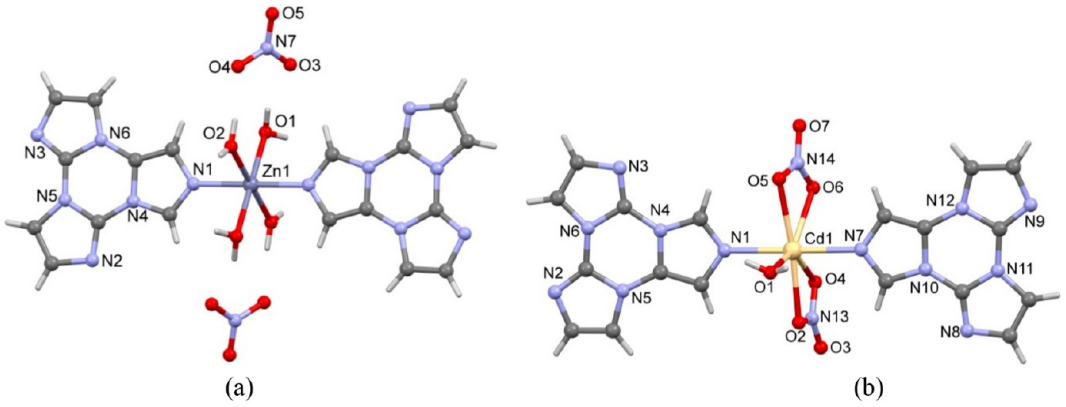

Figure 7. Views of formula units in compounds **8** (a) and **9** (b).

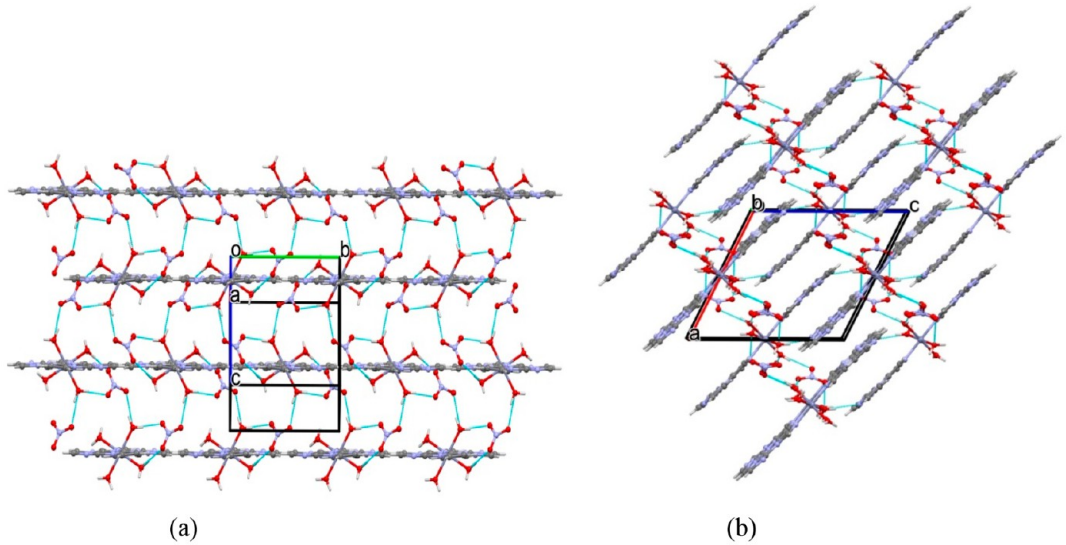

Figure 8. Crystal structure of compound **8**. (a) Fragment of crystal packing along the crystallographic *a* axis showing $OH(H_2O)\cdots O(NO_3^-)$ hydrogen bonds and L_2 pillars placed orthogonally to the supramolecular H-bonded layer; (b) view of crystal packing showing L_2 stacking motif.

$(-x, 1-y, -z)$ = 3.5441(15) Å and Cg(Tr2)···Cg(Tr2) $(-x, 1-y, 1-z)$ = 3.5494(15) Å, while that between dimers, overlapping only through one imidazole ring, is Cg(Im3)···Cg(Im6) $(-x-1, -y, -z)$ = 3.4960(17) Å (Figure S1f).

The centrosymmetric binuclear complex $[Cd_2(bdc)(L_1)_2(NO_3)_2(H_2O)_4]\cdot 2H_2O$ (**7**), obtained as a coprecipitation product in the synthesis of **6**, possesses an extended virtually planar coordination equatorial platform L_1-Cd-bdc-Cd-L_1 which is ∼25.3-Å-long. The Cd(II) atom takes a NO_5 distorted octahedral coordination geometry that comprises the central bidentate chelate bdc anion bridging two Cd(II) atoms, the terminal L_1, two water molecules, and a nitrate anion (Figure 6a). Binuclear complexes are self-assembled *via* $OH(H_2O)\cdots N(L_1)$ hydrogen bonds (Table S2) between coordinated ligands in a stacking layer parallel to the (100) plane where each molecule participates by its three aromatic fragments (L_1, bdc, L_1) in three neighboring stacking columns where the planar moieties alternate in order $L_1\cdots L_1\cdots$bdc$\cdots L_1\cdots L_1$ at rather short stacking distances, Cg(Tr)···Cg(Tr) $(-x, 1-y, -z)$ = 3.807(3) Å and Cg(Tr)···Cg(bdc) $(x-1, y, z)$ = 3.390(3) Å (dihedral angle is 1.8(2)°; Figure 6b). The extended mixed-ligand platform registered in **7** reveals a good opportunity for stacking patterns, while replacement of coordinated water molecules in metal's axial positions opens a further pathway to the mixed-ligand triimidazole-dicarboxylate coordination polymers.

The family of nitrate-containing compounds is complemented by two complexes with the L_2 luminophore, the ionic complex $[Zn(H_2O)_4(L_2)_2](NO_3)_2$ (**8**) and the neutral complex $[Cd(L_2)_2(NO_3)_2(H_2O)]$ (**9**). As with L_1, two L_2 ligands occupy opposite trans positions in metals' coordination cores, and an N atom distal from the triazine core participates in coordination to the metal. The metals' coordination cores are complemented by O-donor ligands, being four water molecules in **8** and two bidentate-chelate nitrate anions and one water molecule in **9**; in both structures, O ligands define the equatorial planes (Figure 7). In compound **8**, the Zn(II) atom takes an octahedral coordination geometry with the N_2O_4 donor set, while in **9** Cd(II) takes a pentagonal−bipyramidal coordination geometry with the N_2O_5 donor set. Ionic complex **8** is centrosymmetric with the Zn atom situated at the inversion center and two L_2 ligands placed in parallel planes. Neutral complex $[Cd(L_2)_2(NO_3)_2(H_2O)]$ resides in a general position; the coordinated L_2 ligands are virtually coplanar, with the L_2/L_2 twisting angle measured as 1.69(7)°.

In **8**, the centrosymmetric complex cations $[Zn(H_2O)_4)(L_2)_2]^{2+}$ and outer-sphere nitrate anions are linked by $OH(H_2O)\cdots O(NO_3)$ hydrogen bonds (Table S2) in supra-

https://doi.org/10.1021/acs.cgd.1c00459
Cryst. Growth Des. XXXX, XXX, XXX−XXX

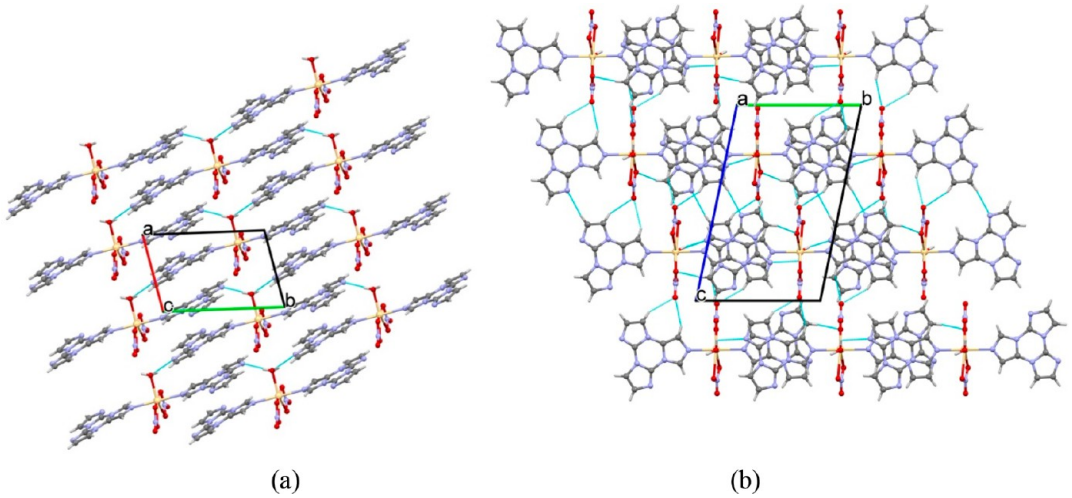

Figure 9. Fragments of crystal packing in **9**. (a) View of stacking layers stabilized by OH(H_2O)···N(L_2) hydrogen bonds; (b) packing of H-bonded layers with indication of CH···O and CH···N edge-to-edge side contacts between neighboring supramolecular layers.

molecular H-bonded layers parallel to the *bc* plane with the L_2 pillars placed orthogonally to this plane (Figure 8a). The supramolecular architecture resembles that of **5** and **6**. Similarly, the L_2 pillars interdigitate in the *ac* plane (Figure 8b). The deep mutual interpenetration of coordinated L_2 ligands is facilitated by OH(H_2O)···N(L_2) hydrogen bonds, which help to bring the luminophores closer and result in L_2 stacking columns where short and long distances between overlapping areas of L_2 alternate, Cg(Tr)···Cg(Tr) ($-x$, $2 - y$, $-z$) = 3.9773(14) Å and Cg(Tr)···Cg(Tr) ($1/2 - x$, $1/2 + y$, $1/2 - z$) = 5.6698(15) Å (Figure 8b, Figure S1g).

In triclinic crystal **9** (Table 1), neutral complexes [Cd(L_2)$_2$(NO_3)$_2$(H_2O)] related by inversion stack in a zipper-like mode along the crystallographic *a* axis being interconnected *via* OH(H_2O)···N(L_2) hydrogen bonds (Table S2) and form H-bonded layers parallel to the (001) crystallographic plane, where L_2 columns alternate with rows of Cd(II) atoms along the *b* axis (Figure 9a). Their stacks are characterized by alternation of rather short distances, Cg(Tr1)···Cg(Tr2) ($x - 1$, $y - 1$, z) = 3.483(4), Cg(Tr1)···Cg(Tr2) (x, $y - 1$, z) = 3.638(4) Å, dihedral angle Tr1/Tr2 = 1.4(3)°, with significant overlapping areas (Figure 9b, Figure S1h). The H-bonded layers are interlinked by CH(L_2)···N(L_2) and CH(L_2)···O(NO_3^-) weak interactions (Figure 9b), thus providing planarization of L_2 motifs in two perpendicular directions.

Two more neutral complexes with L_2, [Zn(L_2)$_2$(CH_3COO)$_2$] (**10**) and [Cd(L_2)$_2$(CH_3COO)$_2$(Im)$_{0.75}$(H_2O)$_{0.25}$]·0.5H_2O (**11**), were obtained from zinc and cadmium acetates. Both crystals are monoclinic (Table 1), and mononuclear complexes reside on the 2-fold axes with interplanar angles between their L_2 wings of 72.51(3)° in **10** and 74.76(4)° in **11**. Despite similarity of the values of dihedral angles between two L_2 ligands, complexes have different shapes: complex **10** has a butterfly shape originated from bending along N–Zn–N, while in **11** the N–Cd–N fragment is linear, the L_2 ligands are twisted along this line, and the complex is no longer of a butterfly shape but resembles a two-bladed propeller.

Similarly to **8** and **9**, L_2 coordinates *via* the distal N atom (Figure 10a,b). The Zn(II) atom takes an N_2O_2 tetrahedral coordination geometry with two acetate and two L_2 ligands coordinated in monodentate modes, while the Cd(II) atom takes an N_3O_4 pentagonal–bipyramidal coordination geometry comprising two bidentate–chelate acetate anions, two monodentate L_2 ligands, and one monodentate Im ligand (75% occupancy); the latter originated from partial degradation of L_2, which alternates in this position with coordinated and outer-sphere water molecules (25% occupancy; Figure S3).

Complexes [Zn(L_2)$_2$(CH_3COO)$_2$] (**10**) form centrosymmetric dimers *via* a couple of CH···N hydrogen bonds (Table S2) giving rise to the $R_2^2(10)$ centrosymmetric homosynthon in the same way as in the L_2 pure form.[6] These dimers form a corrugated H-bonded chain along the crystallographic *c* axis, and chains stack along the crystallographic *b* axis (the shortest in this compound and the shortest crystallographic axis among **1**–**14**, Table 1; Figure 10c) with interplanar separations between L_2 centrosymmetric dimers of 3.424 Å, and alternating short and long distances, Cg(Tr)···Cg(Tr) ($-x$, $-y$, $-z$) = 4.5720(17) Å and Cg(Tr)···Cg(Tr) ($1/2 - x$, $1/2 - y$, $1/2 - z$) = 5.807(2) Å. The stacking layers pack along the crystallographic *a* axis with a herringbone arrangement of adjacent luminophores (Figure 10d). The tetrahedral Zn(II) atom somewhat imitates the tetrahedral geometry of the water molecule in the parent L_2·H_2O structure,[6] similarly providing the herringbone arrangement of the attached luminophores (L_2 stacking ribbons). This results in a stronger rigidification in the coordination network with respect to the pure L_2 structure, due to the replacement of part of hydrogen bonds (with participation of water molecule) by coordination bonds.

Complexes [Cd(L_2)$_2$(CH_3COO)$_2$(Im)$_{0.75}$(H_2O)$_{0.25}$] (**11**) stack along the *b* axis, being interconnected *via* CH···O and OH···O hydrogen bonds (Table S2) with involvement of Im and water molecules alternating in the Cd(II) axial position (Figure 10e, Figure S3). The π–π stacking interactions combine the molecules in π-stacked chains along the crystallographic *a* axis with Cg(Tr)···Cg(Tr) ($3/2 - x$, $1/2 - y$, $-z$) = 4.325(2) (Figure S1j) and interplanar separation of 3.3347(15) Å (Figure 10e). Due to the 2-fold symmetry, the neighboring stacking dimers are oriented in T-shape mode, and the complexes are held together by alternating π–π face-to-face and edge-to-face stacking contacts (Figure 10f).

A one-pot reaction started from zinc chloride resulted in mononuclear complex [Zn(Cl)$_2$(L_1)(H_2O)] (**12**) as block

https://doi.org/10.1021/acs.cgd.1c00459
Cryst. Growth Des. XXXX, XXX, XXX–XXX

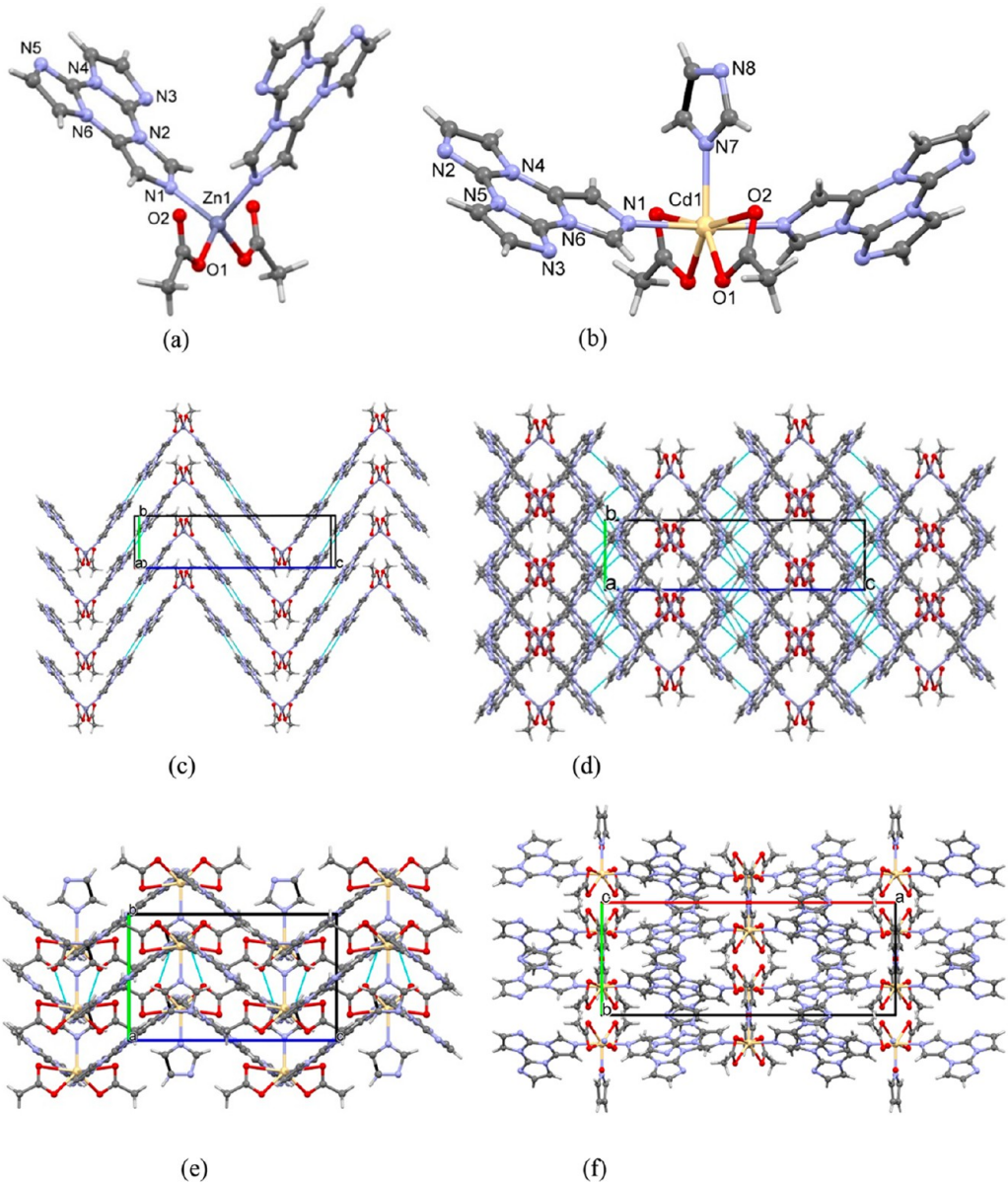

Figure 10. Views of complexes (a) **10** and (b) **11**; (c) view of stacking layer in **10**; (d) crystal packing in **10**; (e) stacking motif in **11**; (f) crystal packing in **11**.

crystals, and one-dimensional (1D) coordination polymer $\{[Zn(Cl)_2(L_1)]\cdot 1/6(L_1\cdot H_2O)\}_n$ (**13**) as needles. Both compounds are noncentrosymmetric (Table 1), and compound **12** crystallizes with two mononuclear complexes per asymmetric unit (Figure 11a). One water molecule from initial salt is replaced by the L_1 ligand in **12**, while complete water replacement in the Zn(II) coordination core occurs in **13**. In the latter structure, L_1 acts as a bidentate bridging ligand affording a 1D coordination chain with a Zn···Zn separation of 7.591(3) Å (Figure 11b). Zn(II) atoms in **12** and **13** take tetrahedral coordination geometries with $NOCl_2$ and N_2Cl_2 donor sets. The mononuclear complex **12** behaves as a double H-donor and a double H-acceptor *via* participation in two $OH(H_2O)\cdots N(L_1)$ hydrogen bonds each (Table S2), thus giving rise to an H-bonded double layer parallel to the *bc* crystallographic plane. Each complex in the layer is linked with three neighbors on the other level (Figure 11c). The long separation Cg(Tr1)···Cg(Tr2) = 5.545(12) Å (L_1/L_1 dihedral angle of 4.8(1)°) between L_1 ligands belonging to different levels of the H-bonded supramolecular layer indicates the lack of meaningful stacking interactions. Layers stack along the crystallographic *a* axis and meet by their hydrophobic L_1 surfaces and Cl atoms from adjacent layers, and no meaningful stacking interactions between the layers are present. The disordering registered in this crystal is explained by the lack of strong intermolecular forces between the layers and resulted in the displacement of the layered motifs, one with respect to the other parallel to the *bc* plane.

The packing of the corrugated polymeric chains in **13** obeys the 3-fold symmetry and is driven by the outer-sphere L_1 ligand that acts as a template and arranges around three coordination chains. These chains pack in a criss-cross mode and are linked with the template L_1 molecule by edge-to-face CH···π interactions. The templated L_1 and water molecules alternate in the channels (Figure 11d).

https://doi.org/10.1021/acs.cgd.1c00459
Cryst. Growth Des. XXXX, XXX, XXX−XXX

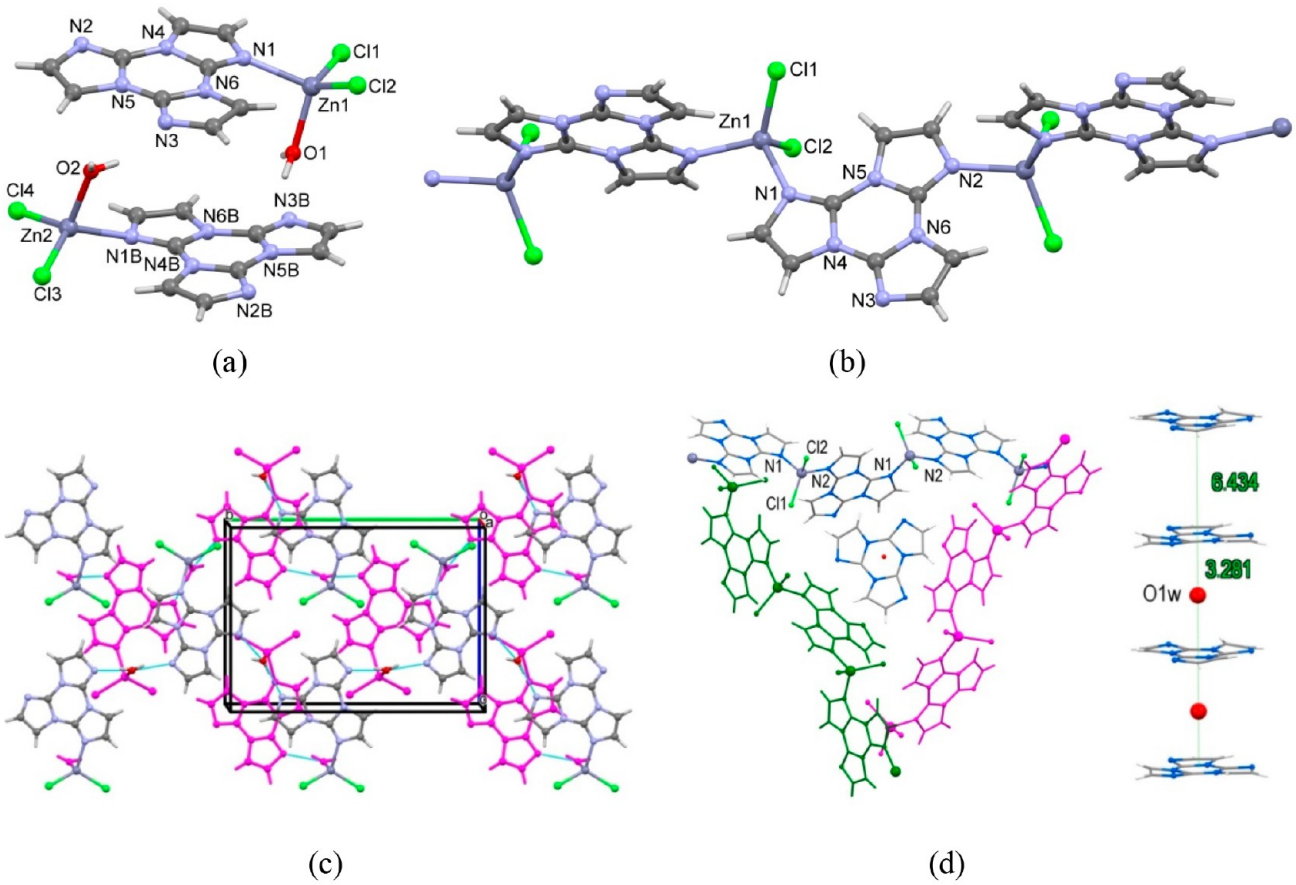

Figure 11. (a) View of mononuclear complexes **12**; (b) fragment of coordination polymeric chain in **13**; (c) fragment of H-bonded double layer in **12** where differently colored complexes belong to different levels; (d) fragment of packing of coordination chains and alternation of templates in the channels in **13**.

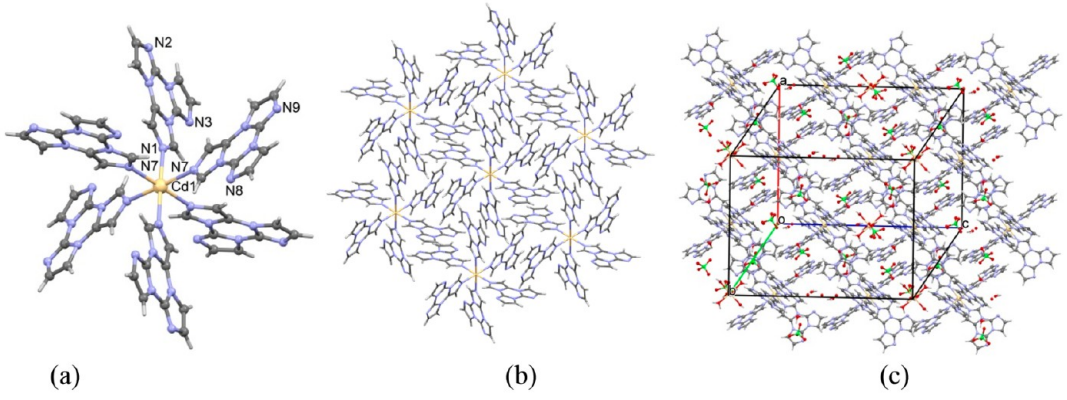

Figure 12. Fragments of crystal packing in **14**. (a) View of $[Cd(L_2)_6]^{2+}$ cations with partial labeling scheme; (b) mode of packing of $[Cd(L_2)_6]^{2+}$ cations indicating π-stacking dimeric patterns; (c) crystal packing with the channels filled by $[Cd(H_2O)_6]^{2+}$ cations, ClO_4^- anions, and water molecules.

Using $Cd(ClO_4)_2{\cdot}6(H_2O)$, with the easy-leaving perchlorate anion, as starting salt facilitates the coordination of six L_2 molecules to the Cd(II) atom resulting in the N_6 octahedral coordination geometry in $[Cd(L_2)_6]_2[Cd(H_2O)_6](ClO_4)_6{\cdot}7(H_2O)$ (**14**). This compound is quite unusual for the metal/ligand 1:6 ratio, indicating that the coordination capacity of the Cd(II) atom is sufficient to arrange six bulky triazine ligands situated in pairs in three perpendicular planes (Figure 12a). Such Cd(II) geometry allows infinite 3D stacking in this crystal, unique in this family of compounds, obtained through two types of very similar centrosymmetric dimers (Figure 12b). The similarity is evident from the close, short Cg···Cg distances, Cg(Tr1)···Cg(Tr1) $(1/3 - x, 2/3 - y, 5/3 - z) = 3.786(4)$ Å and Cg(Tr2)···Cg(Tr2) $(-1/3 - x, 1/3 - y, 4/3 - z) = 3.678(4)$ Å, and alike overlapping areas (Figure S1k). The distinction is connected with capped species perching above these dimers, i.e., ClO_4^- anions and water molecules. $[Cd(H_2O)_6]^{2+}$ cations and ClO_4^- anions act as templates arranging around bulky $[Cd(L_2)_6]^{2+}$ cations in the form of infinite channels (Figure 12c).

https://doi.org/10.1021/acs.cgd.1c00459
Cryst. Growth Des. XXXX, XXX, XXX−XXX

Luminescence Studies. Photophysical studies have been performed for crystals of those compounds revealed as best performing from visual inspection under a UV lamp, namely **4**, **5**, and **10**. All samples display multiple emissions at 298 K (Figures 13−15). The steady state spectrum of compound **4**

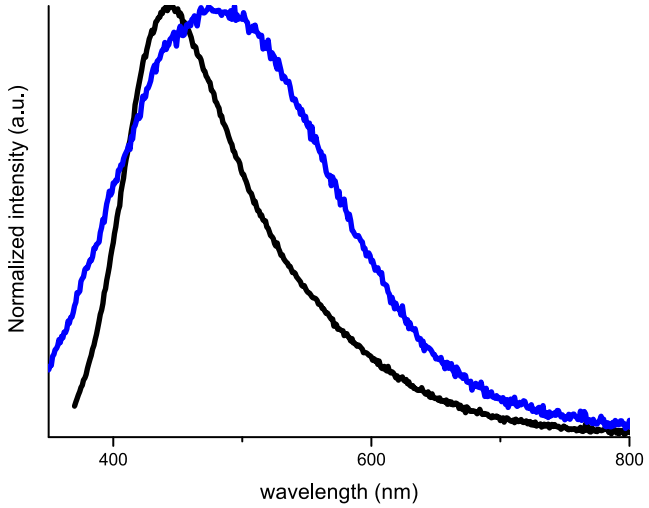

Figure 13. Normalized emission spectra of crystals of **4** at 298 K, black line (λ_{exc} = 350 nm), and 77 K, blue line (λ_{exc} = 330 nm).

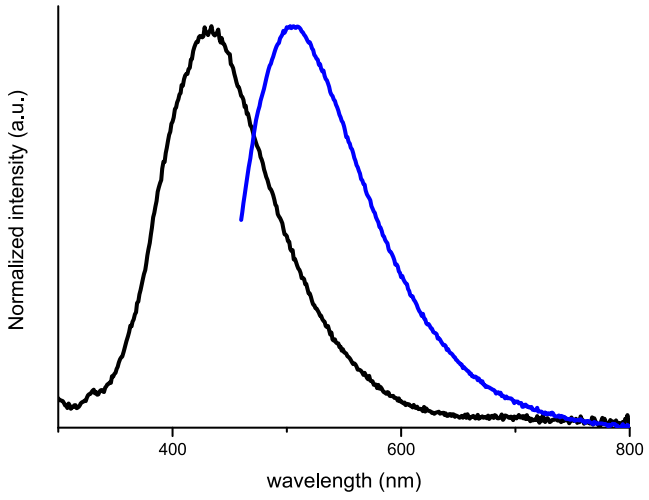

Figure 14. Normalized emission spectra of crystals of **5** at 298 K: black line (λ_{exc} = 280 nm) and blue line (λ_{exc} = 440 nm).

(Figures 13 and S4) is dominated by an intense fluorescence at 439 nm (τ_{av} = 4.36 ns, see Figure S5) with a long-lived tail (τ_{av} = 67.70 ms, see Figure S6) at lower energy (about 550 nm) with overall quantum efficiency Φ = 1%. On the basis of the similarity with the photophysical behavior of other derivatives of L_1, such emissions are of intraligand character, the former associated with molecular fluorescence from S_1 and the latter deriving from π−π aggregate triplet levels. At 77 K, though the two components cannot be resolved (see Figures 13 and S7−S9), the contribution of the phosphorescence is increased as evidenced by the broadening of the emission resulting from the convolution of the two. Comparison with L_1 itself and the previously reported compound $[Zn_3(CH_3COO)_6(H_2O)_2]$-$(L_1)_2$,[35] having a similar organization of L_1 inside the structure but lacking coordination to the metal atom, allows drawing some conclusions on the Zn(II) effect on the photophysical

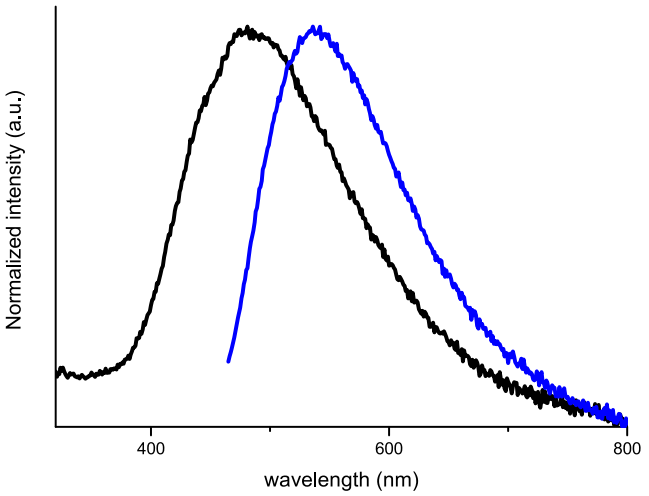

Figure 15. Normalized emission spectra of crystals of **10** at 298 K: black line (λ_{exc} = 300 nm) and blue line (λ_{exc} = 450 nm).

properties of the luminophore. On the basis of the quantum efficiency values and the lifetimes of the long-lived component both decreasing in the order L_1, cocrystal, and **4** (30, 7, and 1%; 970, 650, and 68 ms, respectively), it can be concluded that the presence of Zn(II) facilitates depopulation of S_1 through ISC to a triplet level with $k_r < k_{nr}$, the intrinsic (coordination) effect being more pronounced than the extrinsic (cocrystal) one.

Crystals of compound **5** at 298 K (Figure 14 and Figure S10) show one fluorescence at 430 nm (τ_{av} = 0.61 ns, Figure S11) and a phosphorescence at 505 nm (τ_{av} = 32.69 ms, Figure S12), both of ligand-centered character. In particular, while the former corresponds to radiative deactivation from S_1, the latter is to be attributed to T_1. This assignment is ascribed, on one hand, to the lack of strong π−π interactions between L_1 molecules inside the structure and, on the other hand, to rigidification of the ligand through edge-to-edge CH···N hydrogen bonds which inhibit nonradiative deactivation.

Crystals of compound **10** display at 298 K (Figure 15 and Figure S16) one fluorescence at 490 nm (τ_{av} = 1.94 ns, Figure S17) and a phosphorescence at 550 nm (τ_{av} = 49.29 ms, Figure S18) with overall quantum efficiency Φ = 7%. The absence of strong π−π interactions between L_2 molecules points to a molecular origin (S_1 and T_1) for the two emissions. A greater contribution from the metal with respect to **4** is expected based on the shorter Zn−N(L_2) distance (2.028(3) vs 2.084(2) Å in **10** and **4**, respectively) and confirmed by the appearance of both emissions at low energies.

CONCLUSIONS

Zn(II) and Cd(II) coordination compounds with two isomeric luminophores, namely, triimidazo[1,2-*a*:1′,2′-*c*:1″,2″-*e*][1,3,5]-triazine (L_1) and triimidazo[1,2-*a*:1′,2′-*c*:1″,5″-*e*][1,3,5]-triazine (L_2), are here reported for the first time. The structural landscape comprises mononuclear and binuclear complexes and one 1D coordination polymer. Among them, supramolecular isomers, isostructural compounds, and polymorphs are found. The structural diversity is originated from the different Zn/Cd coordination capacities and results in the variable metal/luminophore/anion/water ratios. In the majority of the reported compounds both luminophores coordinate in the monodentate mode, giving rise to the 1:1, 1:2, and 1:6

https://doi.org/10.1021/acs.cgd.1c00459
Cryst. Growth Des. XXXX, XXX, XXX−XXX

metal/ligand ratios. One example represents the inclusion compound with L_1 associated in the crystal lattice as an outer-sphere stacking dimer. In the 1D coordination polymer, L_1 behaves as a bidentate bridging ligand. The rigidity imposed by coordination of luminophores to the metal centers constrains the ligands in different ways, and the bulky coordination entities with extended heterocyclic platforms generate the diversity of stacking patterns, either similar or not to those registered in the structures of pure forms of L_1 and L_2. The presence of numerous strong H-donors in the form of inner- and outer-sphere water molecules in some complexes provides a significant impact of hydrogen bonding interactions on the crystal packing. Otherwise, a reduced number of water molecules in the system results in a more pronounced impact of weaker intermolecular interactions, such as CH···N hydrogen bonds and $\pi-\pi$ stacking interactions, including those registered in L_1 and L_2 pure forms.

The comparison among L_1, the previously reported cocrystal $[Zn_3(CH_3COO)_6(H_2O)_2](L_1)_2$ and Zn coordination compound $[Zn(L_1)(NO_3)(H_2O)_3](NO_3)$ **4**, having similar stacking arrangement of L_1, provides evidence of the intrinsic/extrinsic heavy Zn(II) metal atom effect on the photoluminescence: the greater the metal contribution, the smaller the quantum efficiency and the shorter the phosphorescence lifetime, both phenomena to be associated with easier ISC.

■ ASSOCIATED CONTENT

Supporting Information

The Supporting Information is available free of charge at https://pubs.acs.org/doi/10.1021/acs.cgd.1c00459.

Tables of selected geometric parameters; figures of L_1/L_2 meaningful overlapping patterns in **1**−**14**, CH···N motifs in polymorphs **5** and **6**, major and minor disordering components in **11**; normalized excitation and emission spectra and lifetime measurements for **4**, **5**, and **10** at 298 and 77 K (PDF)

Accession Codes

CCDC 2076858−2076871 contain the supplementary crystallographic data for this paper. These data can be obtained free of charge via www.ccdc.cam.ac.uk/data_request/cif, or by emailing data_request@ccdc.cam.ac.uk, or by contacting The Cambridge Crystallographic Data Centre, 12 Union Road, Cambridge CB2 1EZ, UK; fax: +44 1223 336033.

■ AUTHOR INFORMATION

Corresponding Authors

Marina S. Fonari − *Institute of Applied Physics, MD2028 Chisinau, Republic of Moldova;* orcid.org/0000-0002-2508-5368; Email: marina.fonari@ifa.md

Elena Cariati − *INSTM-UdR, 20133 Milano, Italy; Dipartimento di Chimica, Università degli Studi di Milano, 20133 Milano, Italy;* orcid.org/0000-0003-1781-0360; Email: elena.cariati@unimi.it

Authors

Victor C. Kravtsov − *Institute of Applied Physics, MD2028 Chisinau, Republic of Moldova*

Victor Bold − *Institute of Applied Physics, MD2028 Chisinau, Republic of Moldova*

Elena Lucenti − *CNR-SCITEC, Institute of Sciences and Chemical Technologies "Giulio Natta", 20133 Milano, Italy; INSTM-UdR, 20133 Milano, Italy*

Daniele Marinotto − *CNR-SCITEC, Institute of Sciences and Chemical Technologies "Giulio Natta", 20133 Milano, Italy; INSTM-UdR, 20133 Milano, Italy*

Alessandra Forni − *CNR-SCITEC, Institute of Sciences and Chemical Technologies "Giulio Natta", 20133 Milano, Italy; INSTM-UdR, 20133 Milano, Italy*

Complete contact information is available at: https://pubs.acs.org/10.1021/acs.cgd.1c00459

Notes

The authors declare no competing financial interest.

■ ACKNOWLEDGMENTS

The authors are indebted for support to the projects ANCD 20.80009.5007.15 (Republic of Moldova) and CNR (Italy)−ASM (R. Moldova) 2018−2019.

■ REFERENCES

(1) Luo, J.; Xie, Z.; Lam, J. W. Y.; Cheng, L.; Chen, H.; Qiu, C.; Kwok, H. S.; Zhan, X.; Liu, Y.; Zhu, D.; Tang, B. Z. Aggregation-induced emission of 1-methyl-1,2,3,4,5-pentaphenylsilole. *Chem. Commun.* **2001**, 1740−1741.

(2) Mei, J.; Hong, Y.; Lam, J. W. Y.; Qin, A.; Tang, Y.; Tang, B. Z. Aggregation-Induced Emission: The Whole Is More Brilliant than the Parts. *Adv. Mater.* **2014**, *26*, 5429−5479.

(3) Mei, J.; Leung, N. L. C.; Kwok, R. T. K.; Lam, J. W. Y.; Tang, B. Z. Aggregation-Induced Emission: Together We Shine, United We Soar! *Chem. Rev.* **2015**, *115*, 11718−11940.

(4) Jin, J.-L.; Geng, Y.; Su, Z.-M. Recent Theoretical Advances in Understanding the Mechanism of Aggregation-Induced Emission for Small Organic Molecules. *Aggregation-Induced Emission: Fundamentals and Applications* **2013**, No. Chapter 18, 399−418.

(5) Yang, J.; Zhen, X.; Wang, B.; Gao, X.; Ren, Z.; Wang, J.; Xie, Y.; Li, J.; Peng, Q.; Pu, K.; Li, Z. The influence of the molecular packing on the room temperature phosphorescence of purely organic luminogens. *Nat. Commun.* **2018**, *9*, 840.

(6) Lucenti, E.; Forni, A.; Botta, C.; Carlucci, L.; Giannini, C.; Marinotto, D.; Previtali, A.; Righetto, S.; Cariati, E. H-aggregates Granting Crystallization Induced Emissive Behavior and Ultralong Phosphorescence from a Pure Organic Molecule. *J. Phys. Chem. Lett.* **2017**, *8*, 1894−1898.

(7) Lucenti, E.; Forni, A.; Botta, C.; Giannini, C.; Malpicci, D.; Marinotto, D.; Previtali, A.; Righetto, S.; Cariati, E. Intrinsic and Extrinsic Heavy-Atom Effects on the Multifaceted Emissive Behavior of Cyclic Triimidazole. *Chem. - Eur. J.* **2019**, *25*, 2452−2456.

(8) Shi, H.; An, Z.; Li, P.-Z.; Yin, J.; Xing, G.; He, T.; Chen, H.; Wang, J.; Sun, H.; Huang, W.; Zhao, Y. Enhancing organic phosphorescence by manipulating heavy-atom interaction. *Cryst. Growth Des.* **2016**, *16*, 808−813.

(9) Gan, N.; Wang, X.; Ma, H.; Lv, A.; Wang, H.; Wang, Q.; Gu, M.; Cai, S.; Zhang, Y.; Fu, L.; Zhang, M.; Dong, C.; Yao, W.; Shi, H.; An, Z.; Huang, W. Manipulating the Triplet Chromophore Stacking for Ultralong Organic Phosphorescence in Crystal. *Angew. Chem.* **2019**, *131*, 14278−14283.

(10) Cornil, J.; dos Santos, D. A.; Crispin, X.; Silbey, R.; Brédas, J. L. Influence of Interchain Interactions on the Absorption and Luminescence of Conjugated Oligomers and Polymers: A Quantum-Chemical Characterization. *J. Am. Chem. Soc.* **1998**, *120*, 1289−1299.

(11) Cornil, J.; Beljonne, D.; Calbert, J. P.; Brédas, J. L. Interchain Interactions in Organic p-Conjugated Materials: Impact on Electronic Structure, Optical Response, and Charge Transport. *Adv. Mater.* **2001**, *13*, 1053−1067.

(12) Xie, Z.; Yang, B.; Li, F.; Cheng, G.; Liu, L.; Yang, G.; Xu, H.; Ye, L.; Hanif, M.; Liu, S.; Ma, D.; Ma, Y. Cross Dipole Stacking in the Crystal of Distyrylbenzene Deriative: The Approach toward High

Solid-State Luminescence Efficiency. *J. Am. Chem. Soc.* **2005**, *127*, 14152−14153.
(13) Qian, Y.; Cai, M.; Zhou, X.; Gao, Z.; Wang, X.; Zhao, Y.; Yan, X.; Wei, W.; Xie, L.; Huang, W. More than Restriction of Twisted Intramolecular Charge Transfer: Three-Dimensional Expanded #-Shaped Cross-Molecular Packing for Emission Enhancement in Aggregates. *J. Phys. Chem. C* **2012**, *116*, 12187−12195.
(14) Xie, Z.; Xie, W.; Li, F.; Liu, L.; Wang, H.; Ma, Y. Controlling Supramolecular Microstructure to Realize Highly Efficient Nondoped Deep Blue Organic Light-Emitting Devices: The Role of Diphenyl Substituents in Distyrylbenzene Derivatives. *J. Phys. Chem. C* **2008**, *112*, 9066−9071.
(15) Cai, S.; Shi, H.; Zhang, Z.; Wang, X.; Ma, H.; Gan, N.; Wu, Q.; Cheng, Z.; Ling, K.; Gu, M.; Ma, C.; Gu, L.; An, Z.; Huang, W. Hydrogen-Bonded Organic Aromatic Frameworks for Ultralong Phosphorescence by Intralayer $\pi-\pi$ Interactions. *Angew. Chem., Int. Ed.* **2018**, *57*, 4005−4009.
(16) Wang, L.; Shen, Y.; Yang, M.; Zhang, X.; Xu, W.; Zhu, Q.; Wu, J.; Tian, Y.; Zhou, H. Novel highly emissive H-aggregates with aggregate fluorescence change in a phenylbenzoxazole-based system. *Chem. Commun.* **2014**, *50*, 8723−8726.
(17) Virgili, T.; Forni, A.; Cariati, E.; Pasini, D.; Botta, C. Direct evidence of torsional motion in an aggregation-induced emissive chromophore. *J. Phys. Chem. C* **2013**, *117*, 27161−27166.
(18) An, Z.; Zheng, C.; Tao, Y.; Chen, R.; Shi, H.; Chen, T.; Wang, Z.; Li, H.; Deng, R.; Liu, X.; Huang, W. Stabilizing triplet excited states for ultralong organic phosphorescence. *Nat. Mater.* **2015**, *14*, 685−690.
(19) Zhang, N.-N.; Sun, C.; Jiang, X.-M.; Xing, X.-S.; Yan, Y.; Cai, L.-Z.; Wang, M.-S.; Guo, G.-C. Single-component small-molecule white light organic phosphors. *Chem. Commun.* **2017**, *53*, 9269−9272.
(20) Yu, J.; Cui, Y.; Xu, H.; Yang, Y.; Wang, Z.; Chen, B.; Qian, G. Confinement of pyridinium hemicyanine dye within an anionic metal-organic framework for two-photon-pumped lasing. *Nat. Commun.* **2013**, *4*, 2719.
(21) Wang, S. Luminescence and electroluminescence of Al(III), B(III), Be(II) and Zn(II) complexes with nitrogen donors. *Coord. Chem. Rev.* **2001**, *215*, 79−98.
(22) Evans, R. C.; Douglas, P.; Winscom, C. J. Coordination complexes exhibiting room-temperature phosphorescence: Evaluation of their suitability as triplet emitters in organic light emitting diodes. *Coord. Chem. Rev.* **2006**, *250*, 2093−2126.
(23) Barbieri, A.; Accorsi, G.; Armaroli, N. Luminescent complexes beyond the platinum group: the d10 avenue. *Chem. Commun.* **2008**, *19*, 2185−2193.
(24) Lustig, W. P.; Li, J. Luminescent metal−organic frameworks and coordination polymers as alternative phosphors for energy efficient lighting devices. *Coord. Chem. Rev.* **2018**, *373*, 116−147.
(25) Medishetty, R.; Nalla, V.; Nemec, L.; Henke, S.; Mayer, D.; Sun, H.; Reuter, K.; Fischer, R. A. A New Class of Lasing Materials: Intrinsic Stimulated Emission from Nonlinear Optically Active Metal−Organic Frameworks. *Adv. Mater.* **2017**, *29*, 1605637.
(26) Wei, Z. W.; Gu, Z. Y.; Arvapally, R. K.; Chen, Y. P.; McDougald, R. N.; Ivy, J. F.; Yakovenko, A. A.; Feng, D. W.; Omary, M. A.; Zhou, H. C. Rigidifying Fluorescent Linkers by Metal−Organic Framework Formation for Fluorescence Blue Shift and Quantum Yield Enhancement. *J. Am. Chem. Soc.* **2014**, *136*, 8269−8276.
(27) Deria, P.; Yu, J.; Smith, T.; Balaraman, R. P. Ground-State versus Excited-State Interchromophoric Interaction: Topology Dependent Excimer Contribution in Metal−Organic Framework Photophysics. *J. Am. Chem. Soc.* **2017**, *139*, 5973−5983.
(28) Yang, X. G.; Yan, D. P. Long-Afterglow Metal-organic Frameworks: Reversible Guest-Induced Phosphorescence Tenability. *Chem. Sci.* **2016**, *7*, 4519−4526.
(29) Rubin, H. N.; Reynolds, M. M. Amino-Incorporated Tricarboxylate Metal−Organic Framework for the Sensitive Fluorescence Detection of Heavy Metal Ions with Insights into the Origin of Photoluminescence Response. *Inorg. Chem.* **2019**, *58*, 10671−10679.
(30) Li, F.; Sun, M.-L.; Zhang, X.; Yao, Y.-G. Diverse Structures and Luminescence Properties of Nine Novel Zn/Cd(II)-Organic Architectures Assembled by Two Different Rigid Ligands. *Cryst. Growth Des.* **2019**, *19*, 4404−4416.
(31) Yin, H.-Q.; Wang, X.-Y.; Yin, X.-B. Rotation Restricted Emission and Antenna Effect in Single Metal−Organic Frameworks. *J. Am. Chem. Soc.* **2019**, *141*, 15166−15173.
(32) Li, Q.; Luo, J.; Wang, L.; Qi, C.; Yang, Y.; Zhang, X.; Qian, J. Two cage-based zinc-tetracarboxylate frameworks with white-light emission. *CrystEngComm* **2017**, *19*, 214−217.
(33) Mercs, L.; Albrecht, M. Beyond catalysis: N-heterocyclic carbene complexes as components for medicinal, luminescent, and functional materials applications. *Chem. Soc. Rev.* **2010**, *39*, 1903−1912.
(34) Lucenti, E.; Cariati, E.; Previtali, A.; Marinotto, D.; Forni, A.; Bold, V.; Kravtsov, V. Ch.; Fonari, M. S.; Galli, S.; Carlucci, L. Versatility of Cyclic Triimidazole to Assemble 1D, 2D and 3D Cu(I) Halide Coordination Networks. *Cryst. Growth Des.* **2019**, *19*, 1567−1575.
(35) Cariati, E.; Forni, A.; Lucenti, E.; Marinotto, D.; Previtali, A.; Righetto, S.; Botta, C.; Bold, V.; Kravtsov, V. Ch.; Fonari, M. S. Extrinsic Heavy Metal Atom Effect on the Solid-State Room Temperature Phosphorescence of Cyclic Triimidazole. *Chem. - Asian J.* **2019**, *14*, 853−858.
(36) Li, R.; Wang, S.-H.; Liu, Z.-F.; Chen, X.-X.; Xiao, Y.; Zheng, F.-K.; Guo, G.-C. An Azole-Based Metal−Organic Framework toward Direct White-Light Emissions by the Synergism of Ligand-Centered Charge Transfer and Interligand $\pi-\pi$ Interactions. *Cryst. Growth Des.* **2016**, *16*, 3969−3975.
(37) Xie, J.; Qiao, J.; Wang, L.; Xie, J.; Qiu, Y. An azomethin-zinc complex for organic electroluminescence: Crystal structure, thermal stability and optoelectronic properties. *Inorg. Chim. Acta* **2005**, *358*, 4451−4458.
(38) Sinha, N.; Stegemann, L.; Tan, T. T. Y.; Doltsinis, N. L.; Strassert, C. A.; Hahn, F. E. Turn-On Fluorescence in Tetra-NHC Ligands by Rigidification through Metal Complexation: An Alternative to Aggregation-Induced Emission. *Angew. Chem., Int. Ed.* **2017**, *56*, 2785−2789.
(39) Yuan, S.; Deng, Y. K.; Sun, D. Unprecedented Second-Timescale Blue/Green Emissions and Iodine Uptake Induced Single Crystal to Single Crystal Transformation in Zn^{II}/Cd^{II} Metal−Organic Frameworks. *Chem. - Eur. J.* **2014**, *20*, 10093−10098.
(40) Cepeda, J.; San Sebastian, E.; Padro, D.; Rodríguez-Diéguez, A.; García, J. A.; Ugalde, J. M.; Seco, J. M. A Zn based coordination polymer exhibiting long-lasting phosphorescence. *Chem. Commun.* **2016**, *52*, 8671−8674.
(41) Luo, F.; Sun, G.-M.; Zheng, A.-m.; Lian, S.-x.; Liu, Y.-l.; Feng, X. F.; Chu, Y.-y. Promising long-lasting phosphor material: a novel metal−organic framework showing intriguing luminescent performance. *Dalton Trans.* **2012**, *41*, 13280−13283.
(42) Malpicci, D.; Lucenti, E.; Forni, A.; Marinotto, D.; Previtali, A.; Carlucci, L.; Mercandelli, P.; Botta, C.; Righetto, S.; Cariati, E. Ag(I) and Cu(I) cyclic-triimidazole coordination polymers: revealing different deactivation channels for multiple room temperature phosphorescences. *Inorg. Chem. Front.* **2021**, *8*, 1312−1323.
(43) Melnic, E.; Kravtsov, V. Ch.; Lucenti, E.; Cariati, E.; Forni, A.; Siminel, N.; Fonari, M. S. Regulation of $\pi\cdots\pi$ stacking interactions between triimidazole luminophores and comprehensive emission quenching by coordination to Cu(II). *New J. Chem.* **2021**, DOI: 10.1039/D1NJ00909E.
(44) Schubert, D. M.; Natan, D. T.; Wilson, D. C.; Hardcastle, K. I. Facile Synthesis and Structures of Cyclic Triimidazole and Its Boric Acid Adduct. *Cryst. Growth Des.* **2011**, *11*, 843−850.
(45) Buck, D. M.; Kunz, D. Triazine Annelated NHC Featuring Unprecedented Coordination Versatility. *Organometallics* **2015**, *34*, 5335−5340.
(46) Sheldrick, G. M. A short history of *SHELX*. *Acta Crystallogr., Sect. A: Found. Crystallogr.* **2008**, *A64*, 112−122.

https://doi.org/10.1021/acs.cgd.1c00459
Cryst. Growth Des. XXXX, XXX, XXX−XXX

(47) Sheldrick, G. M. Crystal structure refinement with *SHELXL*. *Acta Crystallogr., Sect. C: Struct. Chem.* **2015**, *C71*, 3−8.
(48) Macrae, C. F.; Edgington, P. R.; McCabe, P.; Pidcock, E.; Shields, G. P.; Taylor, R.; Towler, M.; van de Streek, J. *Mercury*: visualization and analysis of crystal structures. *J. Appl. Crystallogr.* **2006**, *39*, 453−457.
(49) Spek, A. L. Single-crystal structure validation with the program *PLATON*. *J. Appl. Crystallogr.* **2003**, *36*, 7−13.
(50) Groom, C. R.; Bruno, I. J.; Lightfoot, M. P.; Ward, S. C. The Cambridge Structural Database. *Acta Crystallogr., Sect. B: Struct. Sci., Cryst. Eng. Mater.* **2016**, *B72*, 171−179.
(51) Morris, D. F. C.; MacCarthy, J. D.; Newton, R. J. Outer-sphere and inner-sphere interactions in the formation of metal-ion nitrate complexes. *Electrochim. Acta* **1978**, *23*, 1383−1386.
(52) Etter, M. Encoding and decoding hydrogen-bond patterns of organic compounds. *Acc. Chem. Res.* **1990**, *23*, 120−126.

https://doi.org/10.1021/acs.cgd.1c00459
Cryst. Growth Des. XXXX, XXX, XXX−XXX